ABSTRACT

MOSHER, BRIAN PATRICK. Synthesis and Characterization of Sol-Gel Nanocomposites Demonstrating Enhanced Mechanical Properties. (Under the direction of Taofang Zeng).

The mild reaction conditions of the *sol-gel* process allow incorporation of an *inorganic* component into *organic* materials, making it very favorable for the synthesis of organic-inorganic nanocomposite materials. However, researchers still strive to produce materials with the unique properties of inorganic compounds which also possess the mechanical properties of organic *polymers*. We have developed several sol-gel derived *nanocomposite silicate* materials using both inorganic precursors and organic-inorganic precursors, which show superior mechanical properties due to nanoscale structural reinforcement. The materials reported were developed in three separate investigations, although the synthesis techniques are relatively similar.

STRUCTURAL EVOLUTION OF PARTICLE REINFORCED ORGANIC-INORGANIC WATER-BASED NANOCOMPOSITE MATERIALS

We present for the first time, the use of $Al(ClO_4)_3$, an effective catalyst for synthesis of 3-Glycidoxypropyltrimethoxysilane (GPTMS) - based nanocomposite materials via sol-gel chemistry. Aluminum perchlorate ($Al(ClO_4)_3$) simultaneously serves as catalyst for epoxy polymerization and methoxysilane *hydrolysis* at room temperature. Catalytic effects of Al(ClO4)3 were demonstrated through nuclear magnetic resonance (NMR) of precursor *sols* and structural investigation of resulting films by Fourier transform infrared spectroscopy (FTIR). Our method incorporates nanophase particulate reinforcement; Ludox® TMA

colloidal silica, which possesses surface silanols (Si-OH), further activate the epoxy groups and expedite organic polymerization. The silica nanoparticles chemically link with the organic-inorganic network through Si-O-Si and Si-O-C bonds. Nanoparticles reinforcement serves to strengthen the network and enhance mechanical properties such as microhardness and abrasion resistance while maintaining the unique optical properties of these materials. Furthermore, the synthesis is water-based, providing for an environmentally friendly synthetic route to hybrid materials. We present a general strategy for synthesis of particle reinforced nanocomposite organic-inorganic sol-gels that can serve as a building block for synthesis of more advanced hybrid materials.

PARTICLE-REINFORCED WATER-BASED ORGANIC-INORGANIC NANCOMPOSITE COATINGS FOR TAILORED APPLCATIONS

Based on the concepts in the work described above, we further developed synthetic routes to three organic-inorganic coatings with nanoparticle reinforcement, which serves to enhance mechanical properties. The films are sol-gel derived using *non-ionic surfactant*, with aluminum perchlorate ($Al(ClO_4)_3$) as a catalyst and 3-Glycidoxypropyltrimethoxysilane (GPTMS) as precursor. Through the aid of nanoparticle colloids and a minute amount of catalyst, dense, hard and monolithic materials are obtained. Incorporating metal oxide nanoparticles brings forth unique properties, such as absorbing harmful UV radiation. Silica colloid composites provide greatly enhanced mechanical properties without modifying the unique optical properties of inorganic materials. Water-based synthesis of these coatings is straightforward and produces very few harmful byproducts, making them ideal materials in industry. The materials presented are relatively hard and abrasion resistant with very good adhesion; two of the coatings are UV absorbent. Various colloids can be employed in our

methods to tailor properties and resulting materials may serve applications such as optical, protective, catalytic, guest-host, and multifunctional coatings.

ENHANCING MECHANICAL PROPRETIES OF SILICA AEROGELS THROUGH NANOENGINEERING

Furthermore, we have developed a novel method to prepare modified silica *aerogels*, in which a small amount of water-soluble inorganic synthetic nanocomposite is added (Laponite® RDS). The molecular-level synergism between silica nanoparticles and molecular cross-linkers inverts the relative host-guest roles in glass-polymer composites, leading to new stronger and more robust low-density materials. After drying with supercritical CO_2, the materials were characterized by 3-point bending, transient hotwire techniques, bulk density measurements, transmission electron microscopy (TEM), and Brunauer, Emmett and Teller (BET) method. Transient hotwire methods confirm that the nanocomposite materials retain the ultra low thermal conductivity of pure silica aerogels.

SYNTHESIS AND CHARACTERIZATION OF SOL-GEL NANOCOMPOSITES DEMONSTRATING ENHANCED MECHANICAL PROPERTIES

by

Brian P. Mosher

A thesis submitted to the Graduate Faculty of North Carolina State University in partial fulfillment of the requirements for the Degree of Master of Science in

Mechanical Engineering

Raleigh

2006

Approved by:

Dr. Taofang Zeng **Chair of Advisory Committee**	**Dr. William L. Roberts**
Dr. Angus Kingon **Dept. of Materials Science and Engineering**	**Dr. Fuh-Gwo Yuan**

BIOGRAPHY

Brian P. Mosher was born in Durham North Carolina on November 21, 1981 to parents Ann Elizabeth Walsh Mosher and Earl Franklin Mosher Jr. He graduated from C.E. Jordan High School in 2000 as an academic all American in varsity swimming. He began attending North Carolina State University in the Fall of 2000 and graduated Magna Cum Laud in May 2004, receiving his B.S. in Mechanical Engineering. Brian began his research career as an undergraduate in January 2003 under the direction of Taofang Zeng with a focus on nanocomposite materials, especially those derived through sol-gel chemistry. After receiving his B.S., Brian began graduate studies at North Carolina State University in 2004, continuing his research under Dr. Zeng and will graduate with a M.S. in Mechanical Engineering and a minor in Materials Science in December 2006.

ACKNOWLEDGEMENTS

First I have to give love to my parents Ann and Earl Mosher and thank them for their endless support and guidance. I feel that I have the most fantastic parents a child could ask for and their passion and dedication to my interests will never be forgotten. I would also like to thank my brother, Matthew Mosher, who provided moral and financial support during my humble years as a graduate student. Of course I cannot forget my fabulous friends, especially the BSO, who helped get me through painful years of study. I give a very special thanks to Chunwei Wu, a long time colleague and close friend of mine, who provided support, vast knowledge and experimental assistance during our many years together in the lab. I would also like to thank Nicholas Martin and Benjamin Lawson for their friendship and contribution to the nanocomposite aerogel research. Lastly I would like to acknowledge the many laboratory technicians who provided experimental assistance, with a special thanks to Hanna Gracz (NCSU - Chemistry) for her NMR experimentation and Wallace Ambrose (UNC Chapel Hill, School of Dentistry) for his TEM assistance.

TABLE OF CONTENTS

LIST OF TABLES

LIST OF FIGURES

Chapter 1: Introduction to Sol-gel chemistry and nanocomposite materials

1.1 Introduction to nanomaterials

Nanostructured materials refer to materials whose structural elements – clusters, crystallites or molecules have dimensions between 1 to 100 nm range (1 nm = 10^{-9} m). *Nanomaterials* are synthetic, metastable materials characterized by microstructures in which at least one of their dimensions is less than one hundred nanometers. Using a variety of techniques such as ball milling, sputtering, chemical vapor deposition, lithography, sol-gel formation, scanning tunneling microscopy, and supersonic molecular beams, it is possible to produce materials with dimensions and sizes ranging from a few angstroms to several nanometers. In this work, we will focus on discussion and synthesis of sol-gel derived nanocomposites.

Nanotechnology offers the possibility to fabricate and engineer materials, structures and systems in which the manipulation of the properties and functionalities is a result of controlling material's constituent units – nanoscale building blocks. By controlling the assembly of various nano-objects as building blocks, nanostructured materials can be advantageously engineered to produce unique properties for numerous applications.

When introducing the topic of nanoscale science and nanotechnology, it is traditional to quote from Nobel Prize winner Richard Feynman's lecture entitled "There's Plenty of Room at the Bottom". Feynman proposed using a set of conventional-sized robot arms to construct a replica of themselves, but one-tenth the original size, then using that new set

of arms to manufacture an even smaller set, and so on, until the molecular scale is reached. If we had many millions or billions of such molecular-scale arms, we could program them to work together to create macro-scale products built from individual molecules - a "bottom-up manufacturing" technique, as opposed to the usual technique of cutting away material until you have a completed component or product - "top-down manufacturing".

Nanotechnology is a broad and interdisciplinary area of research and development that has been growing explosively worldwide over the past two decades. It has the potential for revolutionizing the ways in which materials and products are created and the range and nature of functionalities that can be accessed. Nanotechnology is widely considered as the research focus that can directly lead to a series of crucial breakthroughs in science and engineering fields. Nanotechnology will initialize and create revolutionary advances in understanding and application in at least three aspects[1]: breakthroughs in properties that arise from materials fabricated from the nanoscale; synergistic behavior that arises from the combination of unique types of nanoscale materials (i.e. nanocomposites); assembly in nanoscale to realize structure control that can accomplish desirable properties and application.

It is expected that nanotechnology will be developed at three levels: materials, devices and systems. At present, nanomaterials are at the most advanced stage, both in scientific knowledge and commercial applications. Current nanomaterials include multilayers, chains of atoms and atomic clusters on surfaces, quantum dots, three-dimensional nanostructured films, nanoscale materials, and small atomic clusters[2]. Their unique size-dependent properties give these materials superior and controllable properties. There has

already been much progress in the synthesis, assembly and fabrication of nanomaterials, and equally importantly, in the potential applications of these materials in a wide variety of technologies.

1.2 Sol-gel Materials

1.2.1 Overview

Interest in the sol-gel process surged in the early 1980's as researchers sought new routes to prepare conventional ceramics and glasses[3,4,5,6,7]. Sol-gel materials research was motivated by purity of starting materials[8] and lower processing temperatures[9]. Brinker and Scherer, the pioneers of sol-gel chemistry, define sol-gel as "the preparation of ceramic materials by preparation of a sol, gelation of the sol, and removal of the solvent".[4] Although today, the term "sol-gel" has come to encompass systems containing neither true *sols* nor true *gels*, and includes most ceramic synthesis techniques involving dissolved and/or *colloidal* precursors.

In general, the sol-gel process refers to room temperature solution routes for preparing oxide materials. Typically, the process involves hydrolysis and polymerization of metal *alkoxide* precursors of silica, alumina, titania, or zirconia. Sol-gel processing is a form of nanostructure synthesis, as the starting material is a nanoscale unit, a molecule, which undergoes reactions on the nanometer level and results in a material with nanometer features[10]. In the sol-gel process, a homogeneous solution of reactants reacts to form an infinite molecular weight oxide polymer, of which the molecular structure is irreversible. This polymer material is called a *gel*, which is a three-dimensional network

surrounding interconnected pores. The gel is an elastic solid filling the same volume as the initial precursor solution. Ideally, sol-gel derived materials are isotropic, homogeneous and uniform in nanostructure.

When a gel is initially formed, it is called a "wet gel" or "alcogel" as the pores within the gel are filled with alcohol and water. To form the final gel product, the solvent must be removed, typically by dehydrating or supercritical solvent exchange. Dehydrating alcogels results in *xerogels*, which are simply dried open structures. Thermal curing results in densified gels, which are often used as coating materials and thin films. *Aerogels*, which are up to 99% porous and retain a much more open gel structure, can be produced through supercritical solvent exchange (see sections 1.4 and 4.2.2). Maintaining the gel pore structure during drying is often important as the nanostructured pores in gels are the features of greatest interest, both scientifically and technologically. Figure 1.2.1 shows a schematic of various sol-gel processing routes and obtainable products[11]. The organic-inorganic materials presented follow the hydrolysis polymerization, coating, and heating route to obtain dense films. The silica aerogel materials follow the hydrolysis polymerization, gelling, and extraction of solvent route.

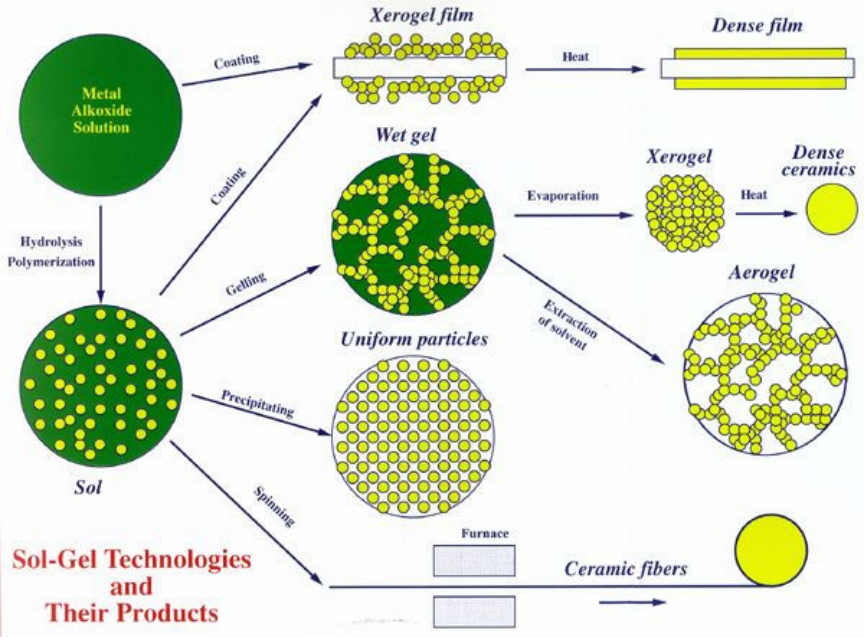

Figure 1.2.1 Sol-gel technologies and their products

Sol-gel nanostructure processing has nearly endless applications because the chemical precursors and synthesis routes can be varied to provide unique properties for specific end uses. As with traditional composites, nanocomposites, which combine advantageous properties of several nanomaterials are proving to be the next stage of materials synthesis. Sol-gel chemistry allows scientists to access an extensive array of precursors and processing techniques so as to fabricate new and exciting materials with controllable structures and properties that can serve applications in almost every aspect of human activity. A chart of various applications of sol-gel derived materials is shown in Figure 1.2.2.

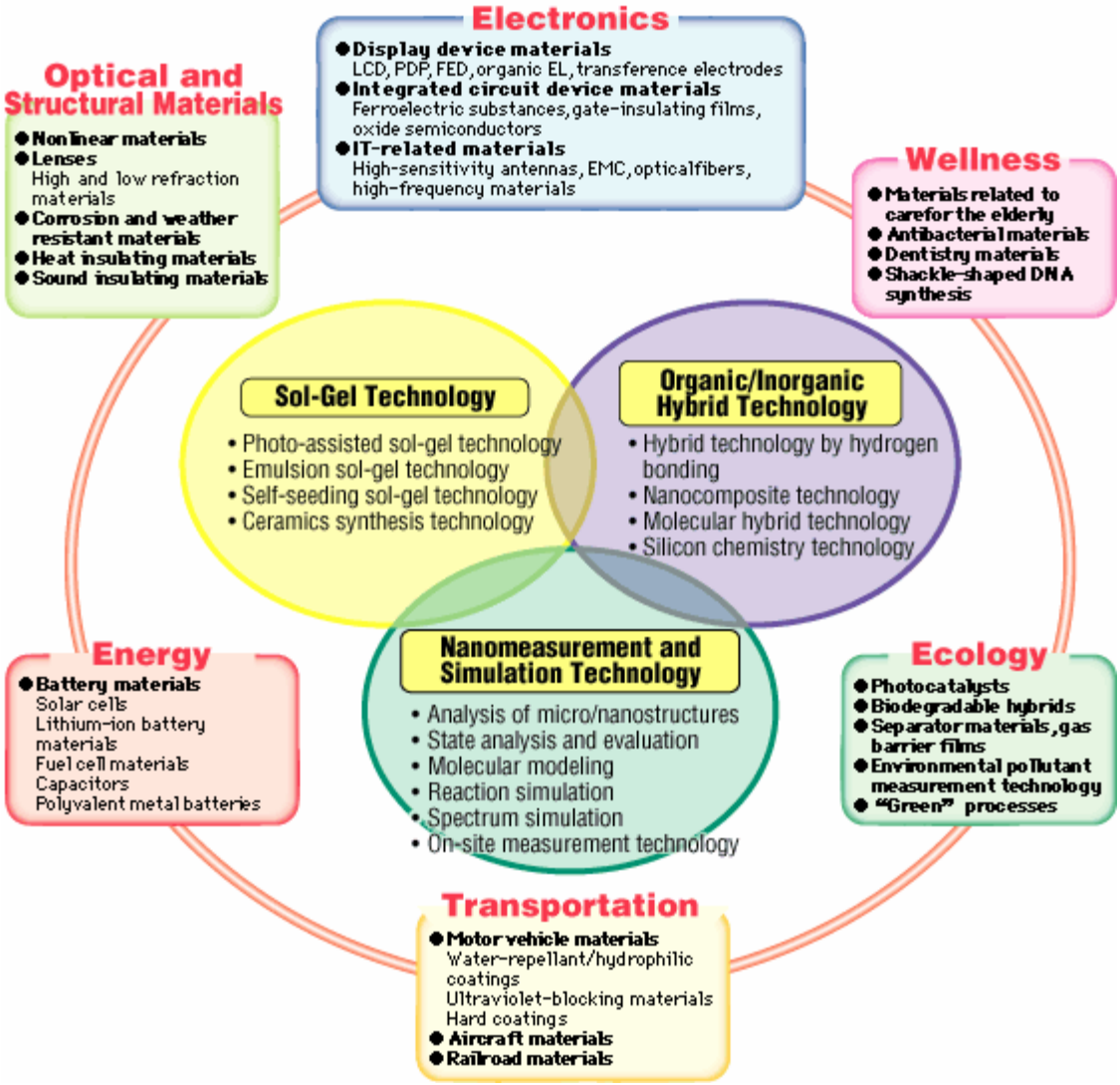

Figure 1.2.2. Applications of sol-gel derived materials[12]

As mentioned, the sol-gel process begins with a homogeneous solution of one or more alkoxides. Many metal alkoxides can be reacted with water through hydrolysis and condensation steps to yield amorphous metal oxide or oxy-hydroxide gels. Metal alkoxides are *metalorganic* compounds, which have an organic *ligand* attached to a metal or metalloid atom. Examples of common alkoxy ligands are listed in Table 1.2.1 (where the dot • indicates an electron that is available to form a bond).

Table 1.2.1 Commonly used alkoxy ligands[4]

Alkoxy	
methoxy	$\bullet OCH_3$
ethoxy	$\bullet OCH_2CH_3$
n-propoxy	$\bullet O(CH_2)_2CH_3$
iso-propoxy	$H_3C(\bullet O)CHCH_3$
n-butoxy	$\bullet O(CH_2)_2CH_3$
sec-butoxy	$H_3C(\bullet O)CHCH_2CH_3$
iso-butoxy	$\bullet OCH_2CH(CH_3)_2$
tert-butoxy	$\bullet OC(CH_3)_3$

In this work we focus on *silicate* based materials, namely those with methoxy- and ethoxy- silane precursors. By far, the most extensively employed sol-gel system is composed of tetraethylorthosilicate [TEOS, $Si(OC_2H_5)_4$], water and alcohol. This is the conventional system to obtain pure silica gels and is discussed further in Section 1.4. The TEOS, water, alcohol system has been employed to synthesize a variety of materials and structures through various sol-gel routes. Sol-gel silicate routes can be varied to produce bulk gels, fibers, films and powders as described in Table 1.2.2. For example, Sakka et al. observed that hydrolysis of TEOS using r (ratio of H_2O / Si) values of 1 to 2 and 0.01 M HCl as a catalyst yields a viscous, spinnable sol (capable of being drawn into a fiber) when aged in open containers exposed to the atmosphere[13].

Table 1.2.2. Sol-Gel Silicate Compositions for Bulk Gels, Fibers, Films and Powders[4]

	mole %					
SiO_2 Gel Types	TEOS	EtOH	H_2O	HCl	NH_3	H_2O / Si
Bulk						
1-step acid	6.7	25.8	67.3	0.2	-	10
1-step base	6.7	25.8	67.3	-	0.2	10
2-step acid-base						
1st step-acid	19.6	59.4	21.0	0.01	-	1.1
2nd step-acid	10.9	32.8	55.7	0.6	-	5.1
2nd step-base	12.9	39.2	47.9	0.01	0.016	3.7
fibers	11.31	77.26	11.31	0.11	-	1.0
films	5.35	36.23	58.09	0.35	-	10.9
Monodisperse spheres	0.83	33.9	44.5	-	20.75	53.61

In typical sol-gel synthesis, a metal alkoxide is combined with water and a solvent (often an alcohol) and the alkoxide reacts with the water. Alkoxysilanes are immiscible in water, however gels can be prepared from silicon alkoxide-water mixtures without additional solvent because the alcohol produced as the by product of hydrolysis is enough to homogenize the initially immiscible system. Typical sol-gel reaction stages are described in the following sections.

1.2.2 Hydrolysis

The reaction of the metal alkoxide with water is called *hydrolysis* because a hydroxyl ion becomes attached to the metal atom, as in the following reaction:

$$Si(OR)_4 + H_2O \rightarrow HO\text{-}Si(OR)_3 + ROH \quad (1)$$

The OR represents an alkoxy group and the ROH is an alcohol. Depending on the amount of water and catalyst present, hydrolysis may go to completion, so that all of the OR groups are replaced by OH:

$$Si(OR)_4 + 4H_2O \rightarrow Si(OH)_4 + 4ROH \quad (2)$$

or, the reaction may stop while the metal is only partially hydrolyzed, $Si(OR)_{4-n}(OH)_n$. Hydrolysis occurs by *nucleophilic attack* of the oxygen contained in water on the silicon atom. Hydrolysis is facilitated in the presence of homogenizing agents like alcohol, which are especially beneficial in promoting hydrolysis of silanes containing bulky organic or alkoxy ligands. However, the presence of solvents may promote esterification or depolymerization reactions according to the reverse of equations (1) and (4).

Hydrolysis is accelerated and more likely to go to completion when *catalysts* are employed[14]. Acid or base catalysts may be employed to promote hydrolysis. Mineral acids such as hydrochloric acid, nitric acid, phosphoric acid, and sulfuric acid, or ammonia are most commonly used in sol-gel processing, although many other catalysts have been employed such as acetic acid, KOH, amines, KF, HF, titanium alkoxides, zirconium alkoxides, aluminum alkoxides, vanadium alkoxides and other oxides. It is widely reported that mineral acids are more effective catalysts than the equivalent concentrations of base. To note, silicon is hydrolyzed even in dilute acid and $Si(OH)_4$ is the predominant mononuclear species below ca pH 7.

1.2.3 Condensation

Partially hydrolyzed molecules then link together in condensation reactions, such as

$$(OR)_3Si\text{-}OH + HO\text{-}Si(OR)_3 \rightarrow (OR)_3\text{-}Si\text{-}O\text{-}Si(OR)_3 + H_2O \quad (3)$$

water condensation

or

$$(OR)_3Si\text{-}OR + HO\text{-}Si(OR)_3 \rightarrow (OR)_3\text{-}Si\text{-}O\text{-}Si(OR)_3 + ROH. \quad (4)$$

alcohol condensation

Condensation, by definition, liberates a small molecule, such as water or alcohol. Under most conditions, condensation begins before hydrolysis completes, thus water condensation and alcohol condensation will typically occur simultaneously. These reactions continue to build larger and larger silicon-containing molecules through polymerization. As with hydrolysis, catalysts are usually employed to induce condensation, although silanols can condense thermally without catalysts. However, to obtain gels with favorable structure, uniform pore size distribution and desirable properties, control of the hydrolysis and condensation rates is required and therefore catalysts are used. Many catalysts have been used for silanol condensation: generally compounds with acid or base character, but also neutral salts and transition metal alkoxides. Mineral acids, ammonia, alkali metal hydroxides, and fluoride anions are typically used[15].

Furthermore, the water : alkoxide ratio, pH, temperature, concentration of the reactants, and the steric and electronic properties of the OR groups, to name only some of the relevant parameters, influence not only the kinetics of the hydrolysis and condensation reactions but also the nano- and microstructure of the obtained oxide.

1.2.4 Gelation

Condensation reactions take place throughout the solution and the alkoxide precursor condenses to form cross-linked polymer particles with an average size of several nanometers. At this point the solution of suspended particles is called a *sol* or

colloid. With monomers that can make more than two bonds there is no limit on the size of the molecule that can form. A *gel* is formed when one molecule reaches macroscopic dimensions so that it extends throughout the solution. The *gel point* is the time at which the last bond is formed which completes the macromolecular gel. When the final bond forms it imparts elasticity to the sol by creating a continuous solid network. This gel network is a continuous solid skeleton which encloses a continuous liquid phase (typically water and alcohol). At the gel point the sol's viscosity rises abruptly and elastic response to stress appears. The sudden change in sol viscosity is used to identify the gel point in a crude way. Often, the *time of gelation*, t_{gel}, is defined as corresponding to a certain viscosity. However, this is misleading because a sharp rise in viscosity may be observed seconds before t_{gel} in one system, but hours before t_{gel} in another system.

In general, the gelation process begins with the formation of fractal aggregates that grow until they impinge on one another, then those aggregates link together as described by *percolation* theory. Percolation theory states that near the gel point, bonds form at random between stationary clusters (polymers or aggregates of particles), linking them together in a network. The gel point relates to the *percolation threshold*, which is when a single cluster (the *spanning cluster*) forms which extends throughout the sol. The spanning cluster reaches across the vessel which contains it, so the sol does not pour when the vessel is tipped. At the moment the gel forms, many clusters are still present in the sol phase, entangled in, but not attached to the spanning cluster. The spanning cluster coexists with a sol phase which contains many smaller clusters, which gradually link with the network. Thus bond formation does not stop at the gel point. The network is initially flexible and compliant, so portions of the gel network can still move close enough

together to allow further condensation. Additionally, there is still a sol within the gel network, so those smaller polymers or particles continue to attach themselves to the network. As the clusters progressively connect to the network, the stiffness of the gel increases. The process of change in structure and properties after gelation is termed *aging*. Thus sol-gel silica polymerization occurs in four stages (as shown in Figure 1.2.2[16]):

1. Polymerization of monomer to form particles.
2. Growth of the particles.
3. Linking of the particles into chains, then networks that extend throughout the liquid medium, thickening it to a gel.
4. Aging of the gel network, with polymeric particles in the sol gradually linking to the network and increasing rigidity and strength.

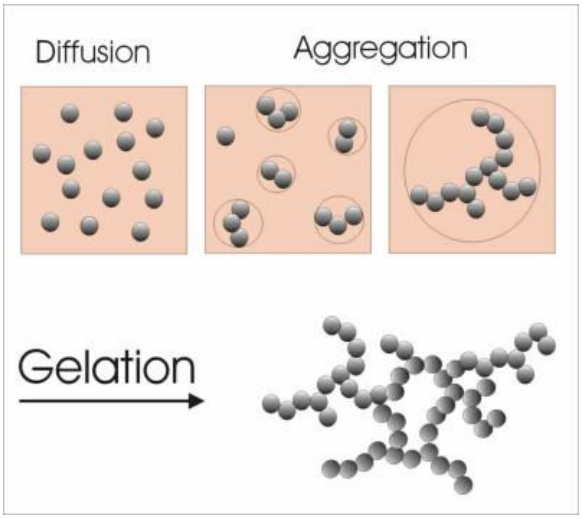

Figure 1.2.3 Stages of sol-gel silica gelation

More recently organic/inorganic metal alkoxide based materials have attracted attention in sol-gel processing due to their unique inorganic properties and favorable mechanical properties resulting from organic incorporation. The organic chains of the

alkoxide precursors can be tailored to unique applications and properties with almost endless possibilities. An introduction to organic/inorganic hybrid materials is presented in section 1.3.

1.3 Organic/inorganic materials

For generations, researchers and human kind alike have sought to combine the properties of different materials. The realization that combining materials can lead to new materials with the beneficial properties of both the constituents led to the development of composite materials, where two different phases with complementary physical properties are combined. The chemical equivalent of traditional composite materials is the combination of chemical groups with different properties on a nanoscale level. Although these nanocomposite materials are macroscopically homogeneous, their properties are born of the chemical building blocks which compose them. The synergic effect created from blending organic and inorganic components in one material allows materials with exceptional properties to be realized. Sol-gel chemistry not only offers an access to ceramics and glasses with improved or unique properties; the very mild reaction conditions, particularly the low reaction temperatures of sol-gel allow incorporation of organic moieties in inorganic materials. Organic/inorganic hybrid polymers are mostly used as coatings with a variety of purposes and constitute the most technically advanced application in the field of sol-gel. These materials are composed of a dual polymer network, in which inorganic polymeric clusters (such as silica) are linked by organic groups or polymer fragments. Such materials combine to some extent the properties of organic polymers with those of metal oxides.

Employing organic groups in sol-gel materials can serve different purposes[17]:

(i) During the preparation of purely inorganic materials, they can control the reaction rates of the reactants, the rheology of the sols, or the homogeneity and microstructure of the derived gels. The organic groups are then degraded by *calcination* to get purely inorganic materials.

(ii) The organic groups can be retained to modify or functionalize the inorganic oxide material. The final material therefore is composed of inorganic structures cross-linked or substituted by organic groups.

In this research, we focus on the second function of organic groups to produce organic-inorganic polymer materials. Hybrid organic-inorganic sol-gel materials can be prepared by two main approaches. Organic molecules can simply be embedded into an inorganic material, or vice versa. Alternatively, the organic and inorganic groupings can be linked by stable chemical bonds. The latter approach requires precursors in which the organic group is bonded to the oxide-forming element (i.e. silicon alkoxide) in a hydrolytically stable way. Today, there exist many *organofunctional* alkoxide precursors which typically contain silicon alkoxide groups at on end linked to one or more functional organic end groups by an organic chain which is covalently bound to the silicon. These organic/inorganic precursors can be reacted through sol-gel processing as to cross-link the monomers to form organic/inorganic polymers.

In the final material, the organic moieties can be located inside the solid or only at its surface. When only one organic substituent in the silicon alkoxide precursor is linked by C-Si bond, the hydrolysis of the Si(OR), group leads to a cross-linked solid in which

most of the organic groups are located at the surface. 3-glycidoxypropyltrimethoxysilane (GPTMS) is one of these precursors and was employed as the organofunctional alkoxide precursor in this work. The GPTMS monomer is shown in the figure below.

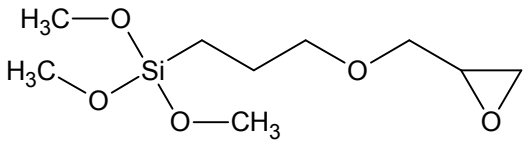

Figure 1.3.1. Molecular structure of GPTMS

Here, the functional organic group is an epoxide ring, which can be opened by catalyst and cross-linked. It should be noted that there exist many organofunctional alkoxides which have been developed over the years to yield specific end use materials with unique, tailored properties arising from specific organic functionalities and structures. Due to the breadth of existing research, these precursors and materials are not discussed and GPTMS-based materials will be considered in detail (see Chapters 2 and 3). It is also interesting to note that for precursors with an aliphatic chain, the specific surface area and the porosities are highly dependent on the length of the chain. Long chains (more than ten CH, groups) lead to solids that behave as resins with no specific surface area or porosity. Under specific conditions, shorter chains (less than ten CH, groups) lead to *mesoporous* solids. The GPTMS chain is relatively short and therefore can produce mesoporous materials with unique structural features.

Typical sol-gel synthesis using organofunctional alkoxides is a two step procedure. First, during sol-gel synthesis, the inorganic alkoxide is reacted through hydrolysis and condensation reactions discussed in section 1.2 and the inorganic network is developed. However, with organofunctional alkoxide precursors, the silica network is initiated with functional organic groups attached. During gelation, the materials can be

molded or applied as coatings with conventional coating techniques (spray, dip, spin-on coating, etc.). Following the sol-gel step, the organic groups are thermally or photo-chemically polymerized or cross-linked to form the organic network. This curing results in permanent hardening of the materials. For example, a highly flexible, nevertheless abrasion resistant coating for polycarbonate was obtained from GPTMS, with l-methylimidazol as the catalyst. 1-Methylimidazol acts as a sol-gel catalyst at room temperature, and in the second step as an initiator for the epoxide polymerization at a higher temperature[18,19]. Due to the different reaction modes of the epoxide group, sol-gel processing of GPTMS can, of course, also be run in a way to deliberately produce diol units. Antifogging coatings on glass were developed by this approach[20].

Alternatively, specific catalysts for organic polymerization can be employed during sol-gel synthesis. Many hybrid materials have been developed using binary alkoxide systems and initiating the silicon alkoxide hydrolysis and condensation in one step and the organic polymerization in a second step. Other syntheses have been developed in which organic and inorganic polymerization occur simultaneously, as in the research presented in this thesis. Researchers have recently shown that in this case of simultaneous polymerization, there is competition between organic and inorganic polymerization. In fact, if the silica network is formed much faster than the organic polymer, the organic chains cannot find enough space to grow and their length is greatly reduced[21]. For this reason, we employ simultaneous polymerization under which the organic groups cross-link more rapidly than the inorganic groups.

1.4 Silica aerogels

Silica aerogels are extremely porous materials synthesized through sol-gel chemistry to form a solvent-filled porous solid, which normally is dried under supercritical conditions in order to prevent collapse of the tenuous solid network. The silicon alkoxide precursor (usually TEOS) undergoes the following hydrolysis and condensation reactions to form a cross-linked, sol-filled porous gel.

Hydrolysis:

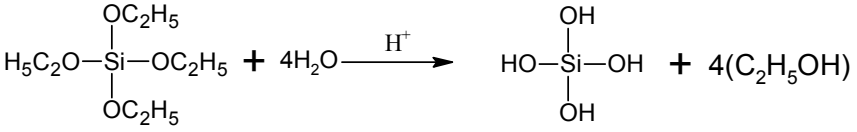

$$TEOS + 4H_2O \longrightarrow Si(OH)_4 + 4(C_2H_5OH)$$

Condensation:

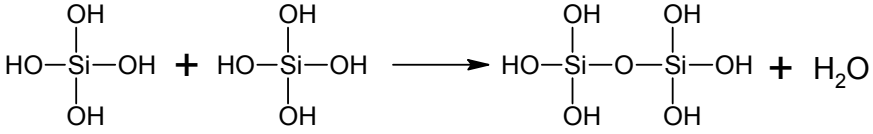

Poly-condensation:

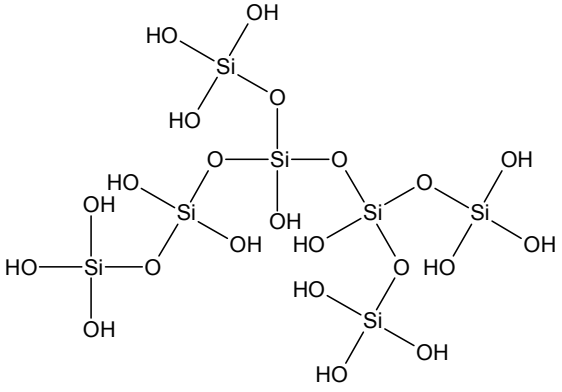

As discussed in section 1.2, when a gel initially forms, it is a solid network surrounding liquid filled pores. To create a vacant porous material, the liquid must be removed from the skeleton. According to Iler, surface forces created in the gel during solvent removal cause the network to collapse as the coordination of the particles is increased[22]. Porosity is achieved when, due to additional cross-linking or neck formation, the gel network becomes sufficiently strong to resist the compressive forces of surface tension. Therefore during drying, the structure which originally formed in solution contracts and distorts and a dried, shrunken xerogel structure results, which comprises both the skeletal and porous phase.

However, through more advanced supercritical solvent exchange techniques, the original pore structure of the gel can be maintained and extraordinarily porous, open structures can be obtained. These materials are called aerogels as they are composed of 90-99.8% air filled pores. Aerogels can be obtained through supercritical drying because removal of a solvent above its critical point occurs with no capillary pressure as there are no liquid-vapor interfaces. Thus the driving force for gel shrinkage is greatly reduced in the aerogel process. Compared with xerogels, aerogels are expanded structures that are often much more closely related to the gel structure formed at the gel point. Although supercritical drying eliminates capillary pressures of the liquid-vapor interfaces, it does not completely eliminate gel shrinkage. In fact, solid-vapor interfaces created at the final stage of supercritical drying can cause weakly condensed gels to shrink up to 50%.

As discussed in section 1.2, the gel structure can be modified by aging after gelation. For all types of gels, aging before solvent extraction can alter the porosity of the dried product[23]. Aging gels in conditions where there is appreciable solubility of the skeletal

phase allows the structure to reorganize via dissolution-reprecipitation reactions. Typically, this will strengthen the gel so that it stops shrinkage earlier in the drying process, causing the resulting aerogels to have greater pore volume.

Some properties of porous materials derived from the different routes described in section 1.2 are listed in Table 1.4.1. These properties are characterized using Brunauer, Emmett and Teller (BET) method in which nitrogen gas is absorbed and desorbed from the porous materials. The two-step acid-base catalyzed method provides the strongest, most highly cross-linked network and is most suitable for aerogel synthesis.

Table 1.4.1. Summary of Porosity of Silicate Xerogels and Aerogels[4]

Sample	Pore Volume (cm^3/g)	Porosity	Surface Area (m^2/g)	Pore Diameter (Å) (absorption)	Pore Diameter (Å) (desorption)	Bulk Density (g/cm^3)
Two-step acid-catalyzed xerogel	345	54%	740	10-50	18	1.54
Two-step acid-base catalyzed xerogel	588	67%	910	10-100	46	0.99
Particulate (one-step base-catalyzed xerogel)	686	70%	515	10-200	125	~0.6
Two-step acid-base catalyzed aerogel	1368	82%	858	10-500	186	0.3

The bulk density, pore volume, pore size and pore size distribution can be varied by varying the synthesis conditions such as catalyst concentrations and type, TEOS, solvent and water ratios, and the aging environment and time. Wagh et al varied the molar ratios of EtOH/TEOS and H_2O/TEOS in order to identify the optimal condition for producing the best quality TEOS silica aerogels in terms of monolithicity, low density and transparency. The molar ratios of EtOH/TEOS and H_2O/TEOS were varied from 2 to 20 and from 4 to 10, respectively. It has been found that lower (< 4) and higher (> 6) EtOH/TEOS ratios result in opaque and cracked aerogels. Wagh et al also found that the gelation time increases and the density decreases with an increase in EtOH/TEOS. On the contrary, lower (< 6) and higher (> 9) H_2O/TEOS ratios resulted in opaque, high density as well as cracked aerogels. It has also been observed that the gelation time decreases with an increase in H_2O/TEOS ratios of above 7 and then it remains almost constant. The density of aerogels decreases with an increase in H_2O/TEOS values up to 9, but further increases in H_2O/TEOS values above 9 lead to an increase in the bulk density of the aerogel. It has been found that EtOH/TEOS values between 3 and 6 and H_2O values between 6 and 9 resulted in monolithic, low density and transparent TEOS silica aerogels.[24]

Aerogels consist of primary particles and pores in the nanometer size range. Numerous unique properties result from their nanostructure and as stated in section 1.2, the pore structure attracts the greatest scientific interest. A typical scanning electron micrscopy (SEM) image of silica aerogel particles and pores is shown in Figure 1.4.1

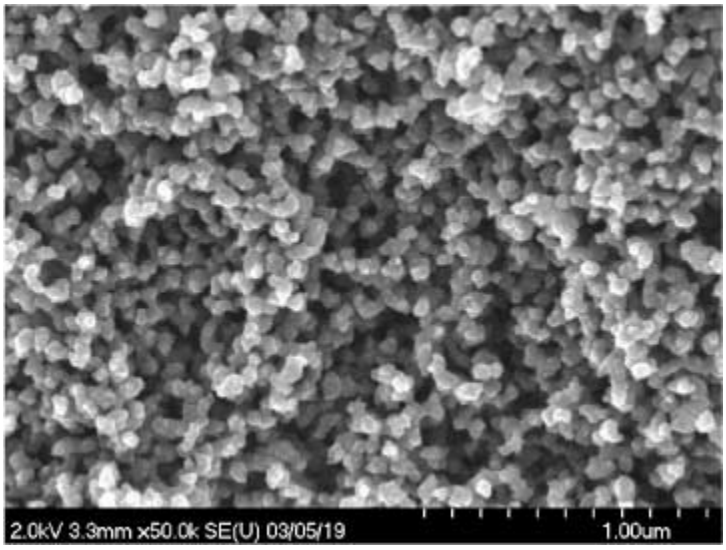

Figure 1.4.1. Scanning electron microscopy (SEM) image of silica aerogel[25]

Arising from their unique nanoporous oxide structure, aerogels exhibit the lowest density, thermal conductivity, dielectric constant and refractive index of any solid material. Due to their high porosity (up to 99.8%)[26] and very large inner surface area (up to 1600 m^2/g)[27] aerogels are used as catalyst supports[28], membranes and reinforcement agents[29], filters for purification of polluted air and water[30], jellifying agents[26a], containers for micrometeorite particles in space[31], and liquid rocket propellants[26b]. They are also being tested in place of CFC blown polyurethane foam, for superthermal insulation in solar energy systems such as solar ponds and cookers, double window panels[32], refrigerators and thermoflasks[33]. Because of their low refractive indices aerogels are used extensively as Cerenkov radiation detectors in nuclear reactors and high energy physics[34]. Since the velocity of sound in silica aerogel is around 100 m/s, they are used as acoustic impedance devices[35]. However, one of the most important and recent applications of silica aerogels is the use of these materials as inertial confinement fusion (ICF) targets in thermonuclear fusion reactions[36]. Recently, silica aerogels have been used as high

efficient radioluminescent light and power sources in place of fragile vacuum systems[37]. Some images of aerogel samples are shown in Figure 1.4.2.

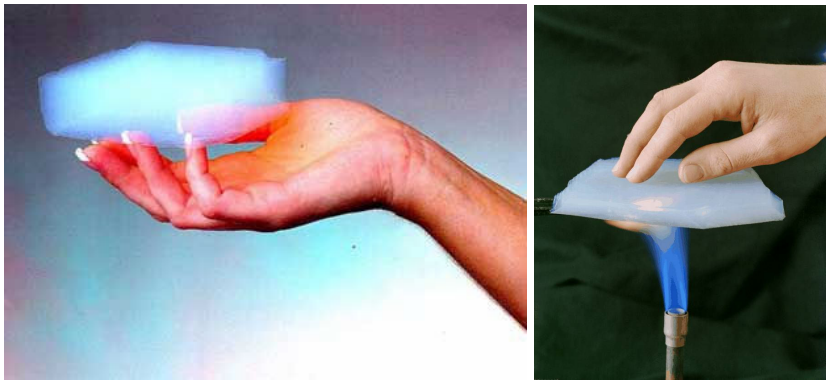

Figure 1.4.2. Images of aerogel samples[38]

Practical application has been slow though, because aerogels are brittle and hygroscopic. Aerogel materials rapidly absorb moisture from the environment, which leads to structural collapse due to the capillary forces that develop in the pores. Improving the poor mechanical properties of silica aerogels has been a topic of study for the past decade. We report the use of Laponite® RDS, a synthetic crystalline silicate, to enhance the mechanical properties of silica aerogels.

Chapter 2: Structural Evolution of Particle-Reinforced Organic-Inorganic Water-Based Nanocomposite Materials

2.1 Introduction

Over the past two decades, researchers have vested interest in organic-inorganic materials based on 3-glycidoxypropyltrimethoxysilane (GPTMS)[39] due to their unique properties and applications as antiscratch coatings[38c], multifunctional coatings[38d], passivation layers for microelectronics[40], and photonic applications serving as host for functional organic molecules[41].

GPTMS contains an epoxy ring, which can be cross-linked to form poly- or oligo-(ethylene oxide) derivatives, thus serving as a network former. Polyethylene oxide (PEO) chains can be induced by ultraviolet or thermal curing[42], or acid or basic catalysts. Basic catalysts include imidazole, methylimidazole (MI), benzylamine, propylamine, poly(oxypropylene)diamine, pyridine and triethylamine. Imidazole and MI show the shortest gelation time amongst these catalysts, suppress bubble formation during drying and produce optically inert materials. Other basic catalysts cause bubble formation during drying, modify optical absorption and/or can degrade nanoparticle additives in synthesis of nanocomposites[43]. Ring opening of GPTMS epoxy rings is traditionally obtained in sol-gel derived materials by *Lewis acids* such as zirconium,[12c,40] titanium[12c,44] or aluminum[45] alkoxides. Although highly effective, such catalysts require addition of *chelating agents* which remain in the microstructure and modify optical properties. The

properties of hybrid materials prepared with these alkoxide catalysts are also highly dependent on the catalyst employed because the alkoxides are co-hydrolyzed with GPTMS and covalently bond with the inorganic network through M-O-Si bonds.

More recently, BF_3OEt_2 was reported as a catalyst for organic polymerization in GPTMS based materials in ambient conditions[46]. Although BF_3OEt_2 shows several advantages over other catalysts, such as shorter reaction times and higher yields, it is highly volatile and careful measures must be taken to avoid the presence of water in the reaction vessel; therefore organic solvent medium is necessary during synthesis. Regardless of the catalyst, until now, nearly all synthesis methods employ organic compounds, leaving the need for more environmentally friendly water-based syntheses unmet.

Ludox® silica particles have been extensively employed in the sol-gel process for synthesis of crack-free mesoporous silicates. Most notable is the method developed by Shoup[47], which employs Ludox® colloid mixed with a potassium silicate solution. The particles act as nucleation sites for precipitation of silicate polymers and microstructure and porosity can be controlled by the percentage of Ludox®. More recently, researchers have shown that GPTMS absorbs on silica nanoparticle surfaces and improves microstructure and mechanical properties of silica colloidal coatings[48].

We present a new water-based, environmentally friendly synthesis route for the preparation of GPTMS based, particle-reinforced nanocomposite materials. We introduce the use of aluminum perchlorate ($Al(ClO_4)_3$) for epoxy ring opening and inorganic hydrolysis at room temperature. Additionally, we employ Ludox® TMA silica colloid as an organic/inorganic polymerization promoter and structural reinforcement.

The synthesis is one step; GPTMS, catalyst and water (or Ludox® TMA) are combined and time is allowed for organic polymerization and sufficient hydrolysis. The substitution of silica colloid for water further promotes epoxy ring opening and expedites inorganic hydrolysis-condensation as well. The silica nanoparticles possess surface silanols, which can additionally react with epoxy rings. During drying the particles split out water to form Si-O-Si bonds and Si-O-C bonds with the network, acting as a chemically bonded particulate reinforcement.

Until now, structural analysis of GPTMS based polymers has been fairly limited and researchers have relied on ^{13}C and ^{29}Si NMR for evaluation. These tools alone cannot fully confirm the polymer architecture. We employ Heteronuclear Correlated Spectroscopy (HETEROCOSY, ^{1}H-^{13}C, one bond and long-range) to confirm structural assignments.

2.2 Experimental Section

Materials. Ludox® TMA Colloidal Silica was purchased from Grace Davison and used as received. 3-Glycidoxypropltrimethoxysilane (97%) and Aluminum Perchlorate Nonahydrate (99%) were obtained from ACROS Organics and used as received. Cleaned silica glass microscope slides and polished aluminum were used as substrates.

Synthesis of Sols. Solutions were prepared for coating, one set with silica colloid ($GPTSiO_2$) and a control set with water (GPT). GPT01, GPT03 and GPT05 were prepared by mixing 5 g GPTMS with 0.1, 0.3 and 0.5 g $Al(ClO_4)_3 \bullet 9H_2O$ respectively, dissolved in 1.14 g H_2O (molar ratio of $Si:Al(ClO_4)_3$ of 1 : 0.1,0.3, and 0.5 respectively). $GPT01SiO_2$, $GPT03SiO_2$ and $GPT05SiO_2$ were prepared by mixing 5 g GPTMS with 0.1, 0.3 and 0.5 g $Al(ClO_4)_3 \bullet 9H_2O$ respectively, dissolved in 1.78 Ludox® TMA silica

colloid. GPTMS:H_2O molar ratio was 1:3 for all sols. Solutions were stirred for one hour in a covered 50 mL glass beaker, then immediately characterized by NMR or were coated on substrates for FTIR and XRD characterization.

Sample Preparation. Coatings were obtained by dip coating fresh sols onto substrates. The samples were either tested as deposited or thermally cured in air at 125°C for 1 hour.

NMR Characterization. Nuclear Magnetic Resonance (NMR) spectra were obtained using a Bruker AVANCE 500 MHz Spectrometer operating at 500.128 MHz for ^{1}H, 125.75 MHz for ^{13}C, 130.32 MHz for ^{27}Al, and 99.36 MHz for ^{29}Si. All NMR scans were performed in CD_3OD, used as received, by mixing the reaction mixtures 1:1 with the solvent. Peak positions were relative to TMS and were calibrated against residual solvent resonance (^{1}H, 3.36 ppm) on the deuterated solvent multiplet (^{13}C, 49.3 ppm). ^{29}Si shifts were measured relative to external TMS with downfield values taken as positive. Two milligrams of chromium (III) acetylacetonate was added as a relaxant for ^{29}Si NMR analysis. The relaxant was found to have no impact on the resulting spectra. ^{27}Al shifts were measured relative to $Al(H_2O)_6^{3+}$ and downfield values were taken as positive. A reference spectra of $Al(ClO_4)_3 \bullet 9H_2O$ was obtained in acetone-d_6 and the intense $Al(H_2O)_6^{3+}$ signal was calibrated to 0.0 ppm.

Infrared Spectroscopy. Fourier Transform Infrared (FTIR) absorption spectra of coating samples were obtained by Attenuated Total Reflectance (ATR) from 4000-650 cm^{-1} using a Nexus 470 FTIR with Avatar OMNI Sampler using a Ge crystal. Solutions were coated on aluminum substrates and were tested as deposited or fired at 125ºC for 1 hour.

X-Ray Diffraction Analysis. X-Ray Diffraction (XRD) analysis was performed on cured films on silica glass microscope slides using a Rigaku D/Max-B X-ray diffractometer (nickel filtered Cu Kα radiation (λ=1.54056 Angstrom) under 35 kV and 30 mA).

UV-Vis Spectroscopy. UV-visible absorption spectra, in the range of 300-800 nm, of films deposited on silica were recorded using a Varian Cary 3 Ultraviolet – Visible Spectrophotometer.

2.3 Results

NMR Spectra. ^{13}C-NMR spectra of various ratios of precursor : catalyst : water were acquired at different reaction times in order to determine the optimum reaction conditions. Silica colloid was substituted for water in order to show its effects on the structural evolution of the gels. ^{1}H-NMR shows little information about the reaction, however ^{13}C-NMR clearly conveys GTPMS polymerization. The epoxy group in GPTMS is characterized by signals at 51.97 and 44.81 ppm of the CH and CH_2 ring carbons respectively. The simultaneous hydrolysis reaction is characterized by the OCH_3 signal at 51.06 ppm. The Si-CH_2-CH_2 carbons produce signals at 6.13 ppm and 23.94 ppm, respectively. The OCH_2 carbons give rise to signals at 74.42 and 72.75 ppm.

Figure 2.3.1 shows ^{13}C-NMR of (1a) GPTMS, (1b) GPT01, (1c) GPT03, and (1d) GPT01SiO_2

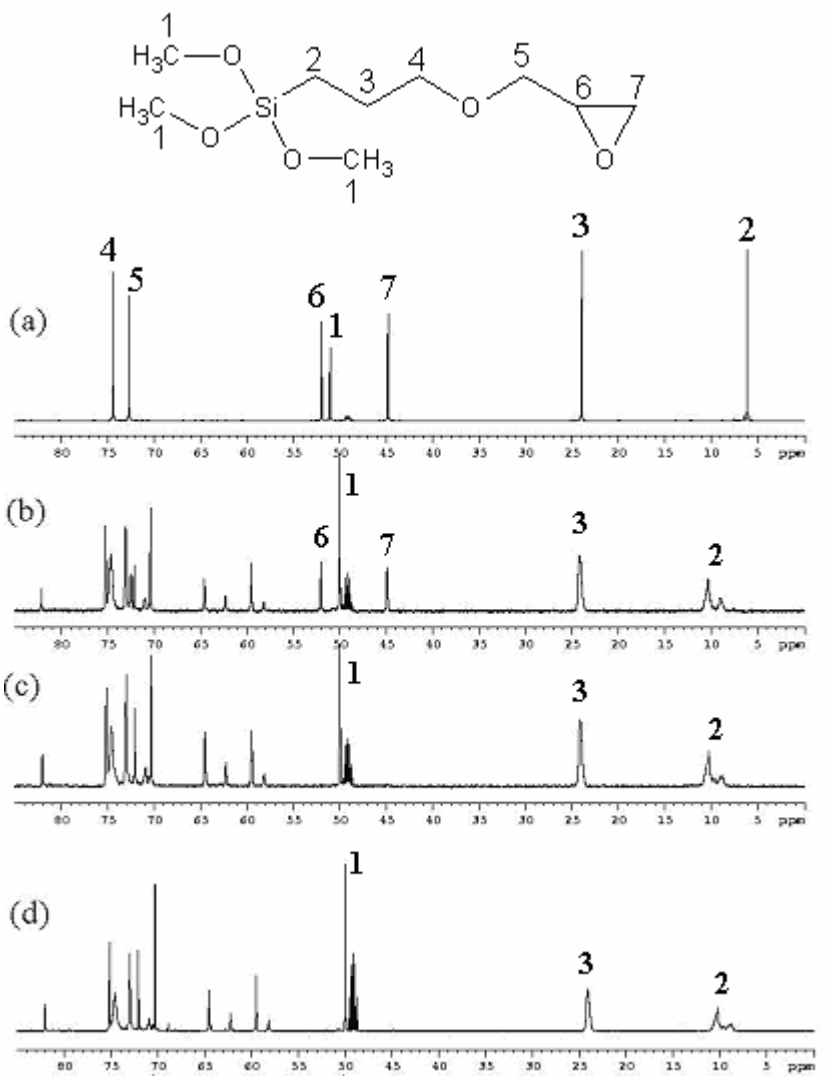

Figure 2.3.1 ^{13}C NMR spectra of (a) GPTMS, (b) GPT01, (c) GPT03 and (d) GPT01SiO2 in the range of 85 to 0 ppm

The GPT01 spectrum (Figure 1b) indicates at least 5% of epoxy rings are still present after 1 hour. The ^{13}C-NMR spectra of GPT03 (Figure 1c) clearly shows simultaneous occurrence of hydrolysis and epoxy ring opening. The characteristic epoxy signals at 51.97 and 44.81 ppm have vanished after one hour reaction time, indicating $Al(ClO_4)_3$ has fully catalyzed the epoxy ring opening and initiated formation of polymer chains. Hydrolysis is indicated by a relatively (to MeOD signal at 49.3 ppm) diminishing

OCH_3 signal at 51.06 ppm. Even with the necessary water for hydrolysis, methyl groups remain on the silicon after one hour; however, subsequent thermal curing completes the reaction through alcohol condensation. A ratio of GPTMS: $Al(ClO_4)_3$ of 1:0.01 does not show complete epoxy ring opening, but as can be seen from the $GPT01SiO_2$ spectrum (1d), when Ludox® TMA is substituted for water, full epoxy ring opening occurs in one hour with $Si:Al(ClO_4)_3$ ratio of 1:0.01. This demonstrates the additional reaction of colloidal silica with the epoxy groups.

Clearly, five new CH_2 groups are distinct in the GPT03 and $GPT01SiO_2$ spectra: δ 75.19; δ 74.60 δ 70.99; δ 64.53; δ 62.28. Four new CH groups also emerge: δ 82.05; δ 72.11; δ 70.56; δ 70.33, along with two new CH_3 groups: δ 59.47; δ 58.14. The GPTMS ether signal at 72.75 ppm has shifted to 73.03 ppm. In samples with Ludox®, a CH also appears at 68.9 ppm. CH_3, CH_2 and CH assignments were confirmed by Distortionless Enhancement by Polarization Transfer (DEPT) (Figure 2.3.2) and 2D ^{1}H-^{13}C NMR.

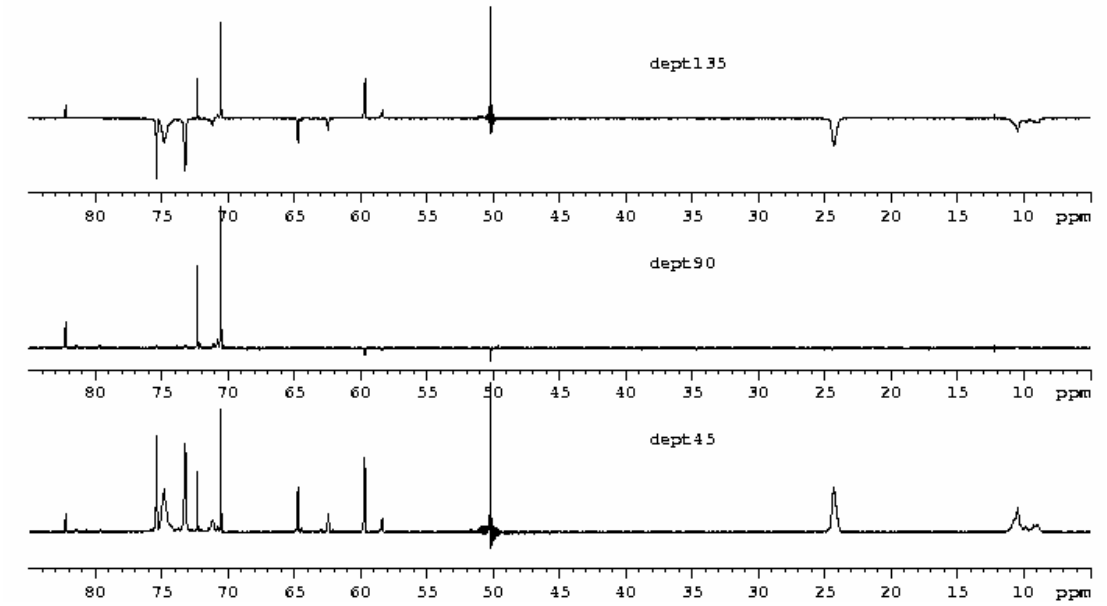

Figure 2.3.2 Distortionless Enhanced Polarization Transfer (DEPT) of GPT03. DEPT45: CH_3, CH_2 and CH upward signals; DEPT90: CH_3 downward signals, CH upward signals; DEPT135: CH_2 downward signals, CH_3 and CH upward signals.

Polymer chain configurations were developed using long-range 2D proton-carbon correlation, which shows neighboring protons up to three bonds from a carbon atom. Detailed assignments are shown in Table 2.3.1. The ^{13}C NMR spectrum of GPT03SiO_2, GPT05 and GPT05SiO_2 (not shown) are quite similar to GPT03 and GPT01SiO_2, showing full epoxy opening. In addition, not only does the silica colloid aid in the epoxy ring opening reaction, it is also seen to expedite inorganic hydrolysis.

Various GPTMS:$Al(ClO_4)_3$:H_2O ratios were also examined. Accordingly, epoxy ring opening is much more strongly related with the ratio of GPTMS:H_2O, than the ratio of GPTMS:catalyst. High ratios of GPTMS:H_2O lead to long reaction times, or high catalyst content for full epoxy ring opening. For example, a ratio of GPTMS:$Al(ClO_4)_3$:H_2O of 1:0.03:3 can open all epoxy rings in one hour. However, when the GPTMS:H_2O ratio is increased to 1:9, a Si:$Al(ClO_4)_3$ ratio of 1:0.2 and 2 hours reaction time are necessary for full epoxy ring opening.

Heteronuclear Correlated Spectroscopy (HETEROCOSY, ^{1}H-^{13}C, one bond and long-range) was employed to assign polymer sequences (Figure 2.3.3 and Figure 2.3.4). The one-bond technique shows the exact position of the protons on each carbon atom and allows us to identify which hydrogen atoms belong to which carbon atoms. Long-range techniques show protons which are less than four bonds from the carbon. This helps infer the relative location of each carbon atom to its neighbor and the specific atomic configurations of the polymer.

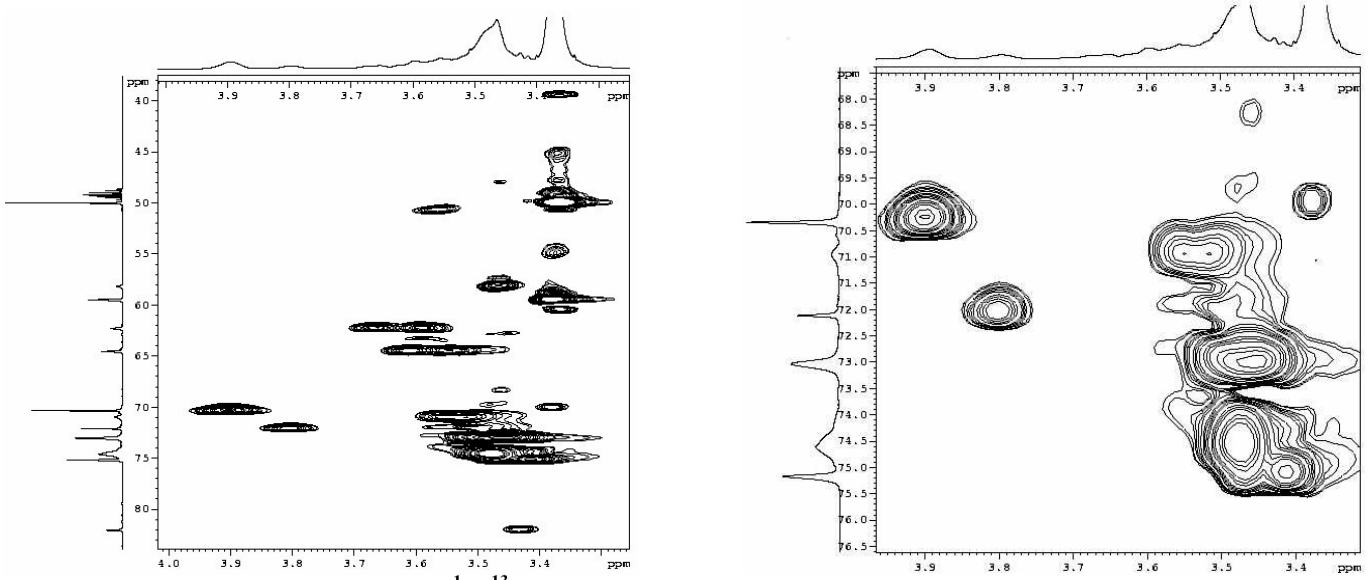

Figure 2.3.3 HETEROCOSY ^{1}H-^{13}C 2-D NMR (one bond) of GPT03. All other 2D spectra of fully reacted solutions are nearly identical. The signal at 68.9 ppm in GPT01SiO_2 and GPT03SiO_2 was too weak to provide clear correlation.

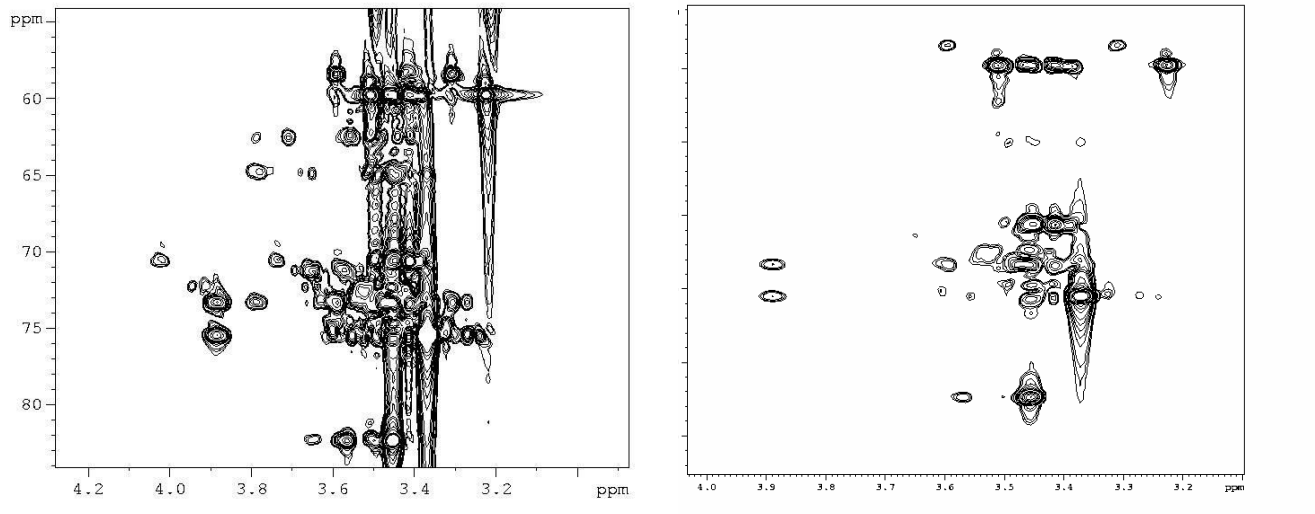

Figure 2.3.4 HETEROCOSY ^{1}H-^{13}C 2-D NMR (long range) of GPT03.
All other 2D spectra of fully reacted solutions are nearly identical.
The signal at 68.9 ppm in GPT01SiO_2 and GPT03SiO_2 was too weak to provide clear correlation.

Unfortunately, even with this powerful tool, it is very difficult to confirm the structural configuration because most of the proton signals are within very close proximity. However, some correlations are quite clear. As expected, the 73.05 ppm (-R-O-$\underline{C}H_2$-) shows long range correlation to nearly every CH and CH_2. The methyl ether at 59.5 ppm (δ_H 3.38) involves the β carbon, which gives rise to the 75.1 ppm signal (δ_H 3.41). The 58.1 CH_3 (δ_H 3.47) shows long range correlation to the 82.0 CH (δ_H 3.43). It is clear that these methyl ethers are formed by the reaction of *diols* with methanol produced from methoxysilane hydrolysis. However, it is apparent that 75.1 CH_2 also represents cross-linking as it correlates with the 74.6 CH_2 protons (δ_H 3.49). The signal at 74.60 ppm is attributed to oligo- and poly(ethylene oxide) derivatives. The 70.33 CH neighbors the 75.1 CH_2 methyl ether or 74.6 CH_2, and also shows bonding to a hydroxyl (δ_H 5.0), indicating it is a CH(OH) in two configurations. The signal appearing at 62.28 ppm may be due to a PEO terminal, but the CH_2 at 70.99 (δ_H 3.55, 3.51) ppm shows clear long range correlation to the 62.28 ppm CH_2 (δ_H 3.66, 3.59) leading us to believe that these signals represent cross-linked -CH_2-O-CH_2-. The 70.99 CH_2 is also quite broad, alluding to its restricted mobility in a cross-linked environment. The carbon signal at 72.1 (δ_H 3.8) is most likely a CH-OH diol, as the 64.5 CH_2(OH) long range correlation shows a proton at 3.8 ppm; however, 72.1 CH correlation to 64.5 C$\underline{H}_2$ could not be confirmed. CH-O-CH_2 cross-linking is also probable, but difficult to confirm. Many of the carbon atoms show long range correlations to protons that could not be identified from one bond 2D NMR. Furthermore the CH signal at 68.9 ppm only appears in the presence of Ludox®, so it is believed to be linked to the surface of the silica nanoparticles.

Table 2.3.1. ^{13}C-NMR assignments from DEPT and HETEROCOSY ^{1}H-^{13}C long range correlations

Assignment	Structural Group	Chemical Shift (ppm)
CH in methyl ether	-R-O-CH_2-**C**H(O-CH_3)-CH_2-O-	82.05
CH_2 in methyl ether and organic/inorganic crosslink	-R-O-CH_2-CH(O-)-**C**H_2-O-CH_3 / Si-O-**C**H_2	75.19
PEO derivatives	-(CH-**C**H_2-O)-$_n$	74.60
CH_2 in ether bridge	-R -O-**C**H_2-CH-	73.03
CH diol	-R-O-CH_2-**C**H(OH)-CH_2(OH)	72.11
Crosslinked CH_2	R-O-CH_2-CH(OH)-**C**H_2-O-CH_2-	70.99
CH-OH (neighboring methyl ether)	R-O-CH_2-**C**H(OH-)-CH_2-O-CH_3	70.33
CH linked with SiO_2 particles	**C**H-O-SiO_2	68.94
CH_2 diol	R-O-CH_2-CH(OH)-**C**H_2(OH)	64.53
Crosslinked CH_2 (neighboring methyl ether)	R-O-CH_2-CH(O-CH_3)-**C**H_2-O-CH_2-	62.28
methyl ether (on CH_2)	R-O-CH_2-CH(O-)-CH_2-O-**C**H_3	59.47
methyl ether (on CH)	R-O-CH_2-CH(O**C**H_3)-CH_2(OH)	58.14

Experiments with only Ludox® and GPTMS under mild heating at 80ºC show a weak 75.1 ppm signal appearing when no methyl ethers are present. This signal may in part be due to PEO linking with surface silanols. Our results show PEO chains are quickly initiated in the presence of Ludox® with no catalyst and mild heating (Figure 2.3.5). However, after a short period of time (~30 min), the epoxy polymerization proceeds very slowly and even after long reaction time, many epoxy groups remain. Furthermore, without $Al(ClO_4)_3$ catalyst, white precipitates form in the solution due to particle agglomeration and homogeneous solutions never result. Films prepared from such solution typically have undesirable morphology and are not transparent or monolithic.

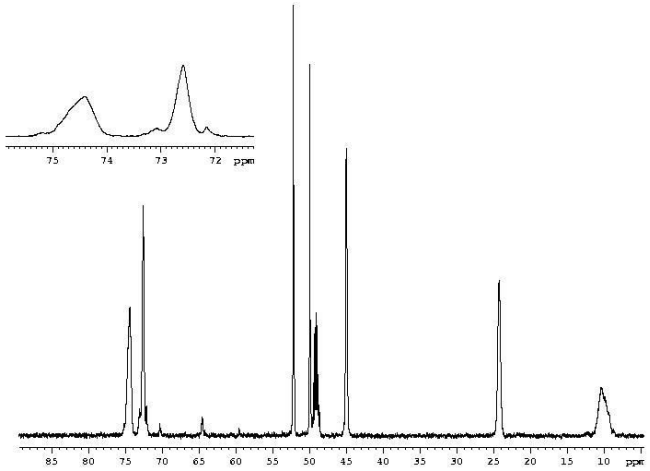

Figure 2.3.5 ^{13}C NMR spectrum of GPTMS+TMA (Si:H_2O 1:3) after 3hrs at 80ºC (in MeOD). Silica colloid has initiated the formation of PEO chains around 74.5 ppm.

^{29}Si NMR spectra of GPTMS and GPT03 are shown in Figure 2.3.6. The GPTMS alkoxide signal (R-Si$(OCH_3)_3$) at approximately -39 ppm is no longer present in the GPT03 spectrum. GPT03 spectrum shows a set of three new complex higher field signals centered at approximately -48.5 (T^1), -56.6 (T^2) and -65 (T^3) ppm. T^1 units

represent those silicon atoms with one siloxane bond, T^2, two siloxane bond, and T^3, three siloxane bonds. The GPT03 spectrum shows a distinct $T^1_{(2OH)}$ signal (R-$Si(OH)_2(O-)$) at -48.5 ppm. The T^2 and T^3 regions show complex, broad signals which arise from the various silicon environments in the extensively cross-linked network. The strongest signal around -56.6 ppm is attributed to $T^2_{(1OH)}$ (R-$Si(OH)(O-)_2$), indicating most methoxysilanes are hydrolyzed, but not fully condensed. The weak T^2 signal around -59.5 ppm is due to R-$Si(OCH_3)(O-)_2$. The signal around -53 ppm is likely due to T^1 (R-$Si(OCH_3)_2(O-)$) as no signals are evident in the T^0 region between -35 to -38 ppm. ^{13}C-NMR show methoxysilane bonds are still present after reaction and ^{29}Si-NMR is in accord as there are two signals which can be attributed to methoxysilanes in the ^{29}Si NMR spectrum. ^{29}Si NMR of GPT01SiO_2 and GPT03SiO_2 are nearly identical to the spectrum in Figure 2.3.6b.

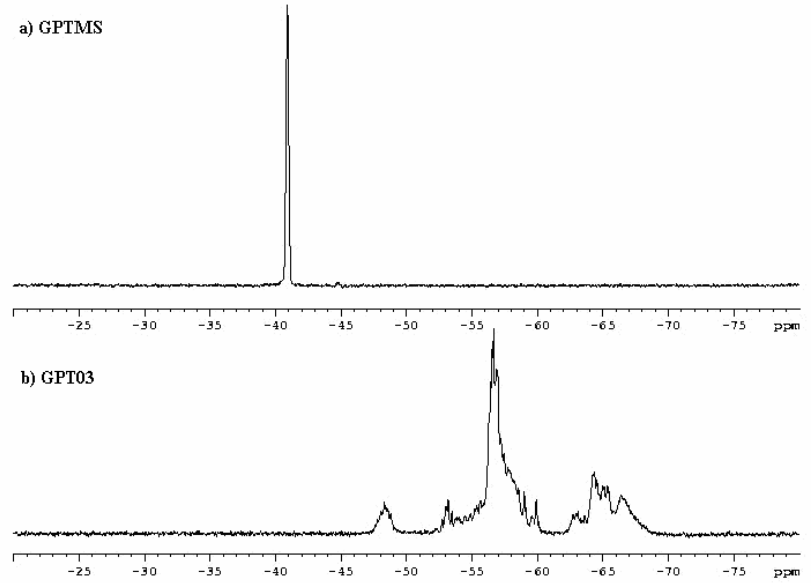

Figure 2.3.6. ^{29}Si NMR spectra of (a) GPTMS, (b) GPT03 in the range of -20 to -80 ppm

^{27}Al-NMR spectra of catalyst $Al(ClO_4)_3$ and GPT03 are shown in Figure 2.3.7a and 2.3.7b respectively. The spectrum in 2.3.7b is representative of all sols. $Al(ClO_4)_3$ in

MeOD displays the sharp $Al(H_2O)_6^{3+}$ signal 0 ppm along with a broad signal at 1.2 ppm and a shoulder at 2.7 ppm. The signal at δ = 1.2 ppm is due to mixed solvates $[Al(H_2O)\bullet(MeOD)_5]^{3+}$ to $[Al(H_2O)_5\bullet(MeOD)]^{3+}$ and the shoulder at 2.7 ppm is due to fac - [$Al(H_2O)_3\bullet(MeOD)_3]^{3+}$ due to coordination with NMR solvent and water in the catalyst[49]. The MeOH coordination is less prevalent in GPT03; the shoulder at 2.7 ppm is no longer present and the signal at 1.2 ppm appears as a shoulder. Due to the additional water present in GPT03, most of the Al^{3+} coordinates with H_2O rather than methanol. There is no evidence that aluminum incorporates into the polymer structure.

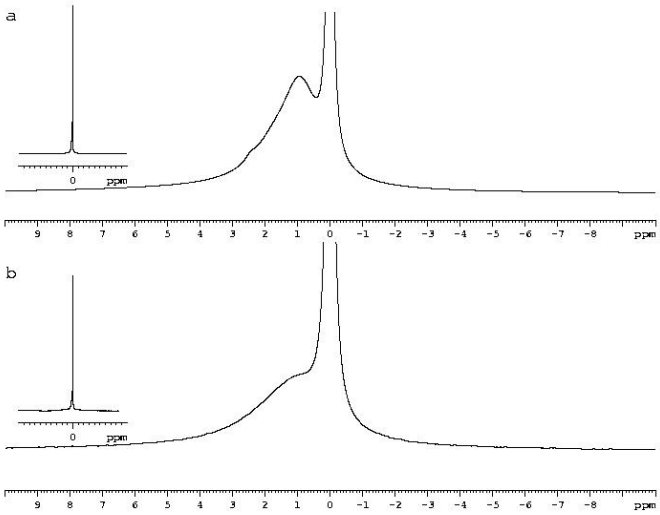

Figure 2.3.7. ^{27}Al-NMR spectra of (a) $Al(ClO_4)_3\bullet 9H2O$ in MeOD and (b) GPT03 in MeOD

FTIR Specta. Epoxy rings show characteristic IR absorption bands at 1251-1241 (ring breathing), 912-920 (asymmetric ring deformation), and 840-853 (symmetric ring deformation) cm^{-1}. The C-H stretch in the epoxy also gives rise to another absorption band at 3065-3038 cm^{-1} [50]. IR spectrum of GPTMS showed epoxy bands peaking at 3050, 1254 and 855 cm^{-1}, which were used as a reference to monitor epoxy ring opening by $Al(ClO_4)_3$.

Figure 2.3.8 shows IR spectra of (a) GPTMS, (b) GPT01, (c) GPT01SiO_2, (d) GPT03 and (e) GPT03SiO_2 from 1000-800 cm^{-1}. It is clear that the epoxy band at 855 cm^{-1} is only evident in GPT01 and has vanished in GPT01SiO_2, GPT03 and GPT03SiO_2. It should be noted that there is also an epoxy absorption band at 910 cm^{-1} (asymmetric ring deformation) in GPTMS. However, this band was seen to increase in intensity after reaction and is present in all samples. As NMR showed full reaction, this signal cannot be due to epoxy deformation in the samples. The broadened and strengthened signal at 910 cm^{-1} is attributed to presence of non-bridging broken free $Si\text{-}O^-$ bonds and the weak band peaking around 970 cm^{-1} is attributed to Si-OH stretching[51]. The absorption band around 820 cm^{-1} in GPTMS, which is due to Si-O(CH_3) symmetric stretching vibration[52], has vanished in all samples indicating hydrolysis has occurred. Hydrolysis is further confirmed by the change in the GTPMS absorption bands at 2940 and 2840 cm^{-1} which are attributed to C-H asymmetric and symmetric stretching in Si-O-CH_3 respectively.

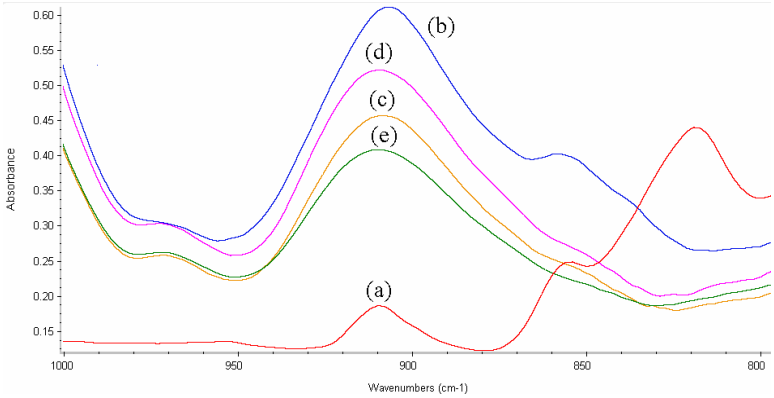

Figure 2.3.8. FTIR normalized spectra of (a) GPTMS (b) GPT01, (c) GPT01SiO2, (d) GPT03 and (e) GPT03SiO2 films deposited on aluminum, between 1000-800 cm^{-1}. Symmetric epoxy ring deformation at 855 cm^{-1}.

Figure 2.3.9 shows spectra of the films in the range of 1300-1220 cm^{-1}. The epoxy ring breathing signal at 1254 cm^{-1} is only evident in GPT01 and has disappeared in the other samples. The epoxy CH_2 stretch seen at 3050 cm^{-1} in GPTMS is not evident in any

of the films (not shown). This further confirms the full epoxy opening in GPT03, GPT03SiO_2 and the effects of silica colloid on epoxy ring opening in GPT01SiO_2.

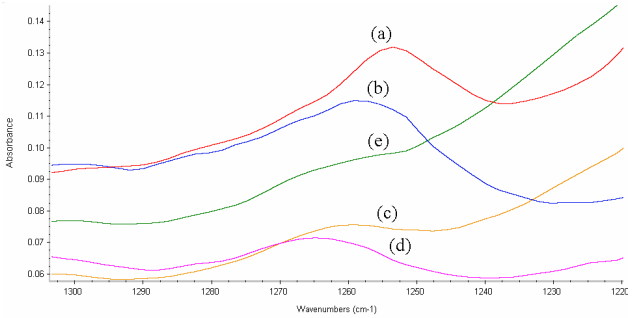

Figure 2.3.9. FTIR normalized spectra of (a) GPTMS (b) GPT01, (c) GPT01SiO2, (d) GPT03 and (e) GPT03SiO2 films deposited on aluminum, between 1300-1220 cm^{-1}. Epoxy ring breathing at 1254 cm^{-1}.

Figure 2.3.10 shows IR spectra of (a) GPT01, (b) GPT03, (c) GPT01SiO_2 and (d) GPT03SiO_2 in the range of 1250-950 cm^{-1}. The spectra are almost identical, showing all bands peaking at similar positions. The strong absorption band around 1090 cm^{-1} is associated with Si-O-Si and Si-O-C asymmetric stretching[53,54]. This peak was found in all samples, however the exact position was seen to vary with catalyst content and silica addition. Si-O-Si peak positions are summarized in Table 2.3.2. Both thermal curing and incorporation of silica nanoparticles shift the Si-O-Si band to higher frequencies, showing that the inorganic network strengthens with both nanoparticles addition and curing[54]. The bands around 1090 cm^{-1}, along with the bands appearing around 1200 cm^{-1} are attributed to Si-O-Si cyclic vibrations. Si-O-Si stretching vibrations in linear and less cross-linked structures give rise to bands around 1120 and 1160 cm^{-1} [17]. These shoulders are not observed in any of the films, indicated highly cross-linked, cyclic structures. The major absorption band is actually composed of three bands at 1090, 1050 and 1027 cm^{-1}. These three band represent a mixture of Si-O-Si, Si-O-C, C-O-C and C-OH bonds. The band at 1027 cm^{-1} is attributed to ν(C-O) and may be due to residual methanol[51a]. However, the

1027 cm^{-1} band is observed even after thermal curing, so it is likely due to CH_2OH or other hydroxyls in the polymers.

Table 2.3.2. Si-O-Si peak positions as a function of catalyst and silica addition. The Si-O-Si position shifts to higher frequencies with increased catalyst, addition of silica colloid and thermal curing.

Sample	as deposited Si-O-Si	Fired 125C Si-O-Si
GPT01	1083.0	1086.7
GPT01SiO_2	1086.6	1089.2
GPT03	1084.1	1094.3
GPT03SiO_2	1089.1	1090.4
GPT05	1085.1	1090.5
GPT05SiO_2	1089.0	1090.9

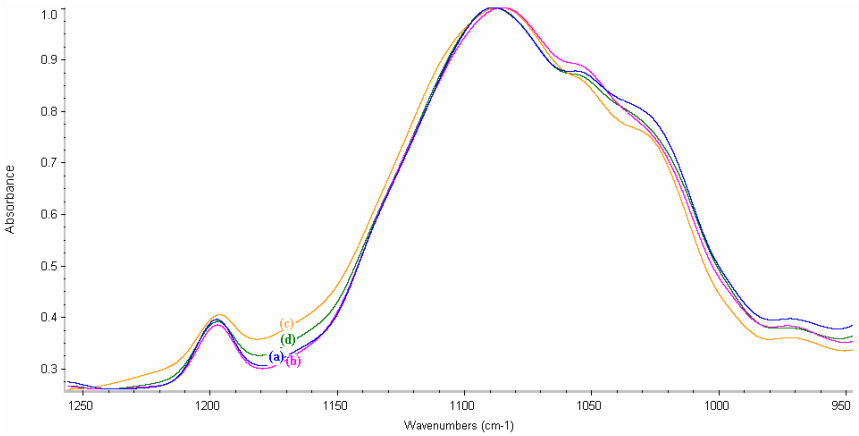

Figure 2.3.10. FTIR normalized spectra of (a) GPT01, (b) GPT03, (c) GPT01SiO_2 and (d) GPT03SiO_2 films deposited on aluminum between 1250-950 cm^{-1}. Si-O-Si cyclic vibrations at 1200 and 1090 cm^{-1} and Si-O-C vibrations at 1090 cm^{-1}. CH_2OH vibrations at 1027 cm^{-1}.

All films, as deposited and fired show broad bands around 3370 cm^{-1} indicating residual surface Si-OH. It should also be noted that the $Si\text{-}O^-$ signal at 910 cm^{-1} is seen to diminish after thermal curing at 125ºC for 1 hour, indicating non-bridging silicon units condense during thermal curing. The 1200 cm^{-1} is also overlapped by the $Si\text{-}CH_2$ wagging vibration band[55]. There is no evidence for the formation of Si-O-Al bonds.

XRD. Figure 2.3.11 shows a representative XRD pattern of GPT03SiO_2 film deposited on silica and fired for 1 hour at 125ºC. XRD patterns of all other films very closely resemble this pattern. The patterns indicate amorphous films with no aluminum precipitates.

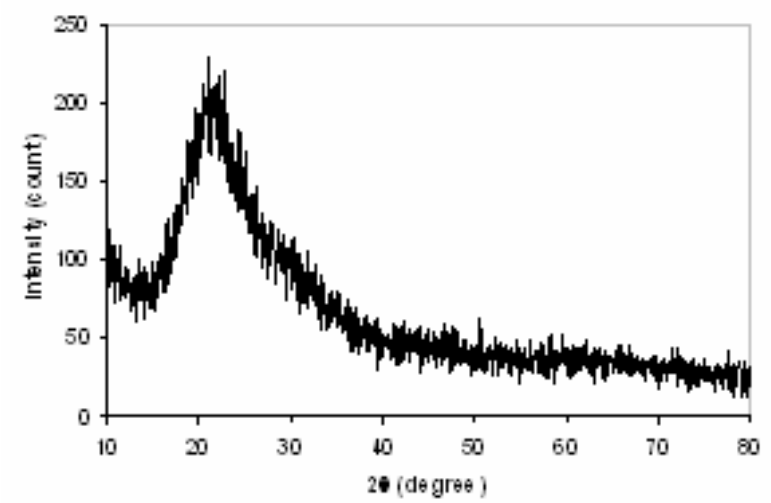

Figure 2.3.11. Representative XRD pattern of GPT03SiO_2 film fired at 125ºC for 1 hour. This pattern is typical for all samples indicating no formation of aluminum precipitates.

UV-Vis Spectra. Figure 2.3.12 shows UV-Vis spectra of (a) GPTMS, (b) GPT01, (c) GPT01SiO_2, (d) GPT03SiO_2 and (e) GPT0GPTMS fired at 125ºC for 1 hour. All films show a longer UV absorption tail than GPTMS and the tail shifts to longer wavelengths with increased catalyst. The GPT01 tail begins around 450 nm and with silica colloid, the GPT01SiO_2 tail is shifted to above 500 nm. GPT03 and GPT03SiO_2 show tails shifted upwards of 600 nm. The tail shift to higher frequencies is indicative of a strengthened, more highly cross-linked network. Furthermore, there is no significant visible absorption bands in any of the films showing that the optical properties are unaffected by the catalyst or silica nanoparticles.

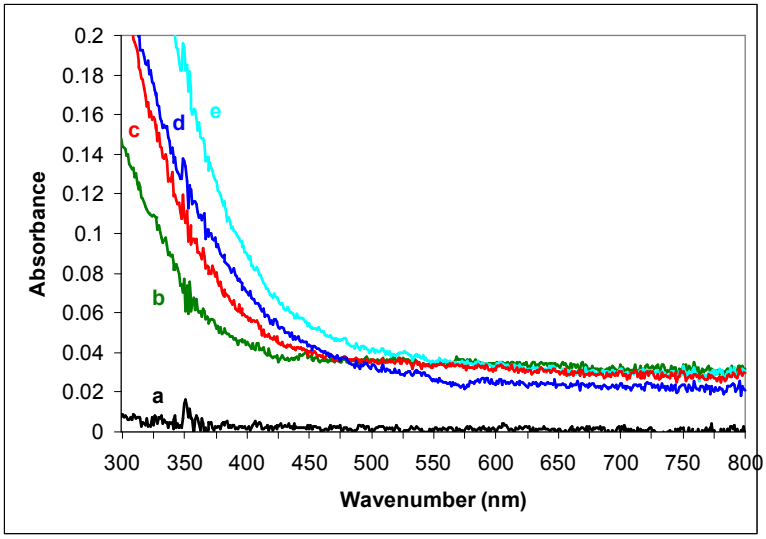

Figure 2.3.12. UV-Vis spectra of (a) GPTMS, (b) GPT01, (c) GPT01SiO_2, (d) GPT03SiO_2 and (e) GPT03 films fired at 125ºC for 1 hour, in the range of 800-300 nm.

2.4 Discussion

Acid or base catalysts can be employed for hydrolysis and condensation reactions in sol-gel processing of GPTMS based materials, although specific catalysts must be selected for epoxy polymerization. Epoxy ring-opening polymerization can be achieved by cationic, anion or covalent nucleophilic mechanisms. Here, $Al(ClO_4)_3$ is employed for both epoxy polymerization and inorganic hydrolysis. Epoxy ring opening is achieved by $Al(ClO_4)_3$ *nucleophilic attack* as shown in Scheme 2.4.1. NMR and FTIR show $Al(ClO_4)_3$ to be an effective catalyst for epoxy opening in ambient conditions. Polymerization can occur due to attack at both the α (Scheme 2.4.1, route b) and β carbons (Scheme 2.4.1, route a)[56]. Products from the C_β attack are favored, however as ^{13}C-NMR and HETERCOSY NMR show, a complex mixture of PEO derivatives is formed. As shown by NMR and IR experiments, Ludox® TMA further promotes epoxy polymerization, also by nucleophilic attack of surface silanols.

There are four possible reactions of the epoxy group. The epoxy ring can either react (1) water, resulting in a diol (Scheme 2.4.2), (2) methanol from inorganic hydrolysis, resulting in methyl ethers (Scheme 2.4.3), (3) another epoxy, resulting in oligo- or poly(ethylene oxide) chains (Scheme 2.4.4), or (4) Si-OH groups, forming Si-O-C bonds (Scheme 2.4.5), either with the silicon atoms of the precursor, or on the surface of silica nanoparticles[53,57]. All products are evident from NMR and FTIR spectra, although it is difficult to clearly confirm Si-O-C bonding by NMR. It is also likely that diols or hydroxyls condense with each other and/or with silanols during drying and thermal curing. Indeed IR shows $Si\text{-}O^-$ (910 cm^{-1}) groups condense during thermal curing.

Scheme 2.4.1

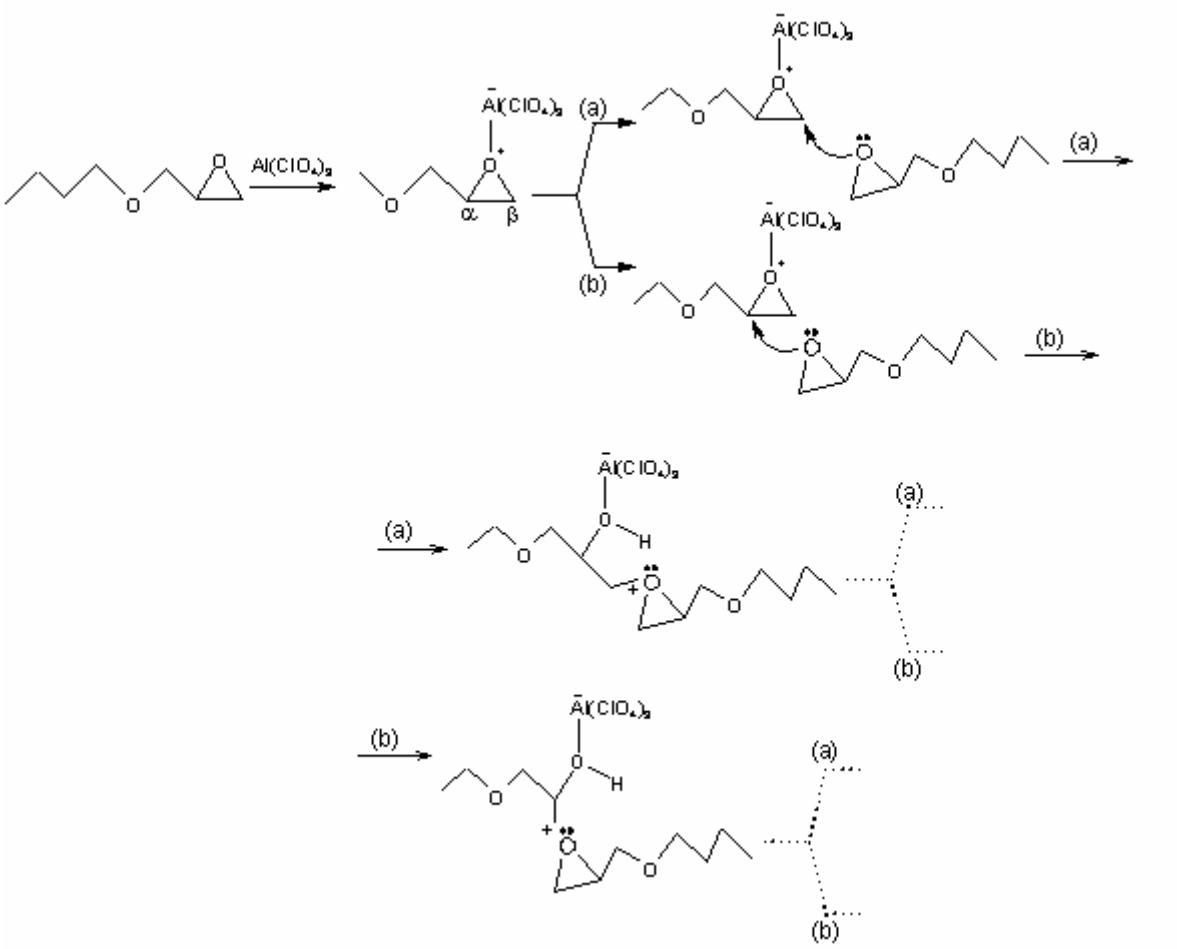

Scheme 2.4.2

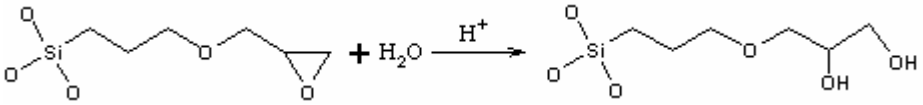

Scheme 2.4.3

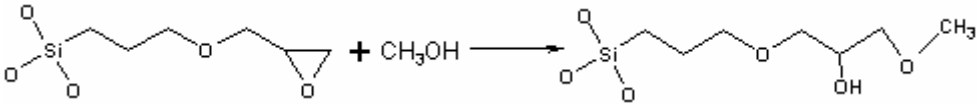

Scheme 2.4.4

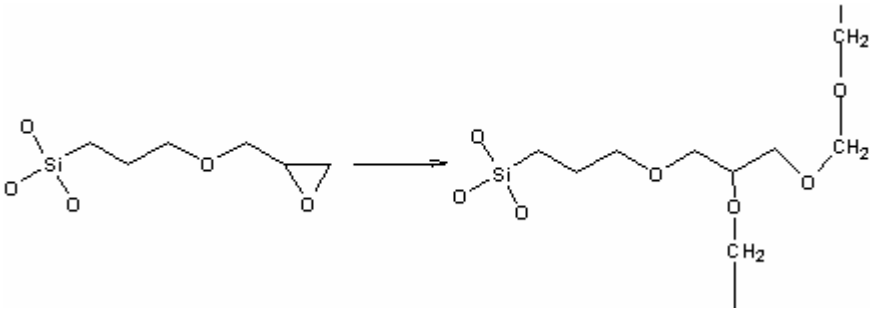

Scheme 2.4.5

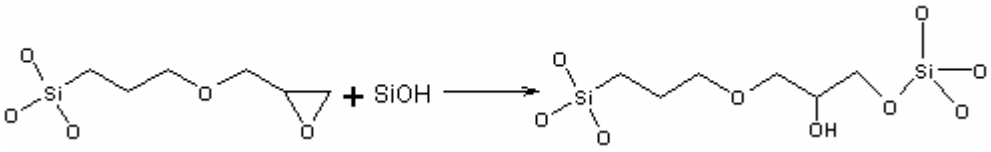

Aside from Si-CH_2-CH_2, no upfield signals appear in the ^{13}C NMR spectra, indicating all other carbons are bound to oxygen atoms, either as ethers, alcohols (i.e. diol) or Si-O-C. Two methylether CH_3 carbons are clearly identified at about 59.5 ppm and 58.1 ppm, indicating that either methanol reacts with the epoxies at both the α and β positions, or diols react with methanol from inorganic hydrolysis forming CH-O-CH_3 and CH_2-O-CH_3 methyl ethers[50,51a,58]. It is unfavorable for methanol to react with epoxy at the α position, so the CH methyl ether is most likely due to methanol reacting with an already formed diol. A CH_2 diol is distinct at 64.5 ppm[59] and in the presence of $Al(ClO_4)_3$, diols form regardless of water content. The complex group of signals 70-75 ppm indicate organic cross-linking and the formation of oligo- and poly(ethylene oxide) derivatives and likely Si-O-C bonds. The reaction also significantly alters the Si-CH_2-CH_2 and CH_2-O-CH_2 patterns. Broadening of the CH_2 groups adjacent to the Si atom at 10 and 24 ppm is indirectly indicative of its restricted mobility, implying inorganic condensation has occurred[52a]. The broadened and shifted OCH_2 signal at 73.03 ppm also shows chemical shift anisotropy, indicating its limited rotation, implying organic cross-linking. The broad CH_2 signal at 74.60 is attributed to the formation of oligo- and poly(ethylene oxide) chains[18,60] and is overlapping the OCH_2 signal in the GPTMS ether bridge.

In addition, the broad Si-CH_2 signal around 10 ppm, along with signals in ^{29}Si NMR spectra are actually complex sets of several signals, implying that the silicon units

are in multiple configurations, which include different degrees of Si-O-Si condensation (including bonding to particle surface), Si-OH, Si-O-CH_3 bonds and possibly Si-O-C cross-linking. The various silicon environments are confirmed by ^{29}Si NMR, which shows the presence of T^1, T^2 and T^3 siloxane bonds, along with silanols and residual methoxysilanes and likely Si-O-C as well. However, it is impossible to definitively identify organic-inorganic cross-linking even with 2D long-range correlation, because the $\underline{H_2}$C-O-Si-C$\underline{H_2}$ protons are four bonds from either carbon. Although ^{13}C NMR shows that silica nanoparticles expedite epoxy ring opening, the reaction rate of Si-OH + Si-OH condensation is much faster than the reaction of Si-OH + epoxy[54]. Therefore, few of the silanols will react with the epoxies and Si-O-C bonds may be present but undetectable. It is likely rather that the organic chains absorb on the surface of the silica particles. Indeed a CH signal at 68.9 ppm only appears in the presence of Ludox®. Si-H HETEROCOSY was attempted but no long range correlations could be detected.

IR further implies the formation of Si-O-C bonds between organic/inorganic chain terminals and/or between epoxies and silica nanoparticles, showing Si-O-Si, C-O-C and Si-O-C vibration bands between 1100-1000 cm^{-1}. Silanols on the nanoparticles also expedite inorganic polymerization by reacting with unhydrolyzed $SiOCH_3$ through silanolysis or alcohol condensation. When catalyst and Ludox® are added to GPTMS, the exothermic hydrolysis and epoxy reactions heat the solution to 70-80°C, providing conditions for Si-OH + Si-O-CH_3 condensation. Comparing IR of samples with and without silica colloid, all samples containing the colloid show Si-O-Si bands at higher frequencies, indicating stronger, more highly cross-linked networks.

GPT05 and GPT05SiO_2 typically react quickly resulting in a solid gel within a few minutes. GPT03SiO_2 often reacts to gelation within one hour as well. Therefore when GPTMS:H_2O is 1:3, a ratio of GPTMS:$Al(ClO_4)_3$ less than 0.03 should be used for coating applications. GPT01SiO_2 provides the best viscosity for film preparation. Higher GPTMS:H_2O ratios also provide suitable coating sols, however require significantly higher catalyst content and longer reaction times. It is visibly observably that when Ludox® is substituted for water, polymerization occurs much more rapidly and the sol's viscosity is much greater.

All sols were soluble in alcohol and acetone, or mixtures of alcohol and water and can be further diluted for film preparation. The advantage of this straightforward, ambient preparation route is that it can be tailored to make unique materials for advanced optical, protective, catalytic or guest-host applications. Surfactants, surface additives, or other nanophase materials can easily be incorporated to the synthesis route. We have developed coating solutions based on this strategy which employ a very minimal amount of catalyst, very high water content and various nanoparticle colloids, allowing for a long-shelf life material, ideal in commercial application[61] (these materials are discussed further in Chapter 3). With these materials, complete reactions do not occur in a short period of time, but organic/inorganic polymerization is achieved during drying and thermal curing. Furthermore, the catalyst and colloid content can be adjusted to synthesize pre-reacted coating sols, which only require short thermal curing times. Drying and subsequent UV-irradiation can also be employed and a dense, hard, abrasion resistant and transparent material is achieved through our water-based route.

2.5 Summary

$Al(ClO_4)_3$ has demonstrated excellent catalytic properties for epoxy opening and subsequent organic polymerization in GPTMS water-based solutions. Substitution of silica colloid for water reduces required catalyst amount and reaction times and produces homogeneous materials with favorable properties. The results demonstrate the formation of Si-O-Si and C-O-C bonds and suggest Si-O-C bonding as well. It is clear that epoxy polymerization can indeed be achieved through a water-based route and although diols and methyl ethers are formed, extensive cross-linking still occurs. HETEROCOSY ^{1}H-^{13}C NMR has been employed to evaluate polymer architecture and confirm many previously unknown chemical environments. The use of water rather than solvents leads to a more environmentally synthesis route.

Chapter 3: PARTICLE-REINFORCED WATER-BASED ORGANIC-INORGANIC NANCOMPOSITE COATINGS FOR TAILORED APPLCATIONS

3.1 Introduction

In recent years, federal regulations have become stricter on Hazardous Air Pollutants (HAPs) and Volatile Organic Compounds (VOCs), creating higher demand for cleaner and safer synthesis of coatings. Water-based coatings create very low VOCs and virtually no HAPs, making them ideal materials in industry. Further, when applying water-based coatings, equipment can be cleaned much more easily, without the use of solvents or other chemicals.

We present a new water based environmentally friendly synthesis route for the preparation of 3-glycidoxypropyltrimethoxysialen (GPTMS)-based, particle-reinforced nanocomposite materials with aluminum perchlorate ($Al(ClO_4)_3$) as catalyst for organic/inorganic polymerization. Three materials were developed: $GPSiO_2$, $GPCeO_2$ and GPCeZr which are reinforced with colloidal silica, cerium oxide, and zirconium and cerium oxides, respectively. $GPSiO_2$ synthesis is a one-pot, two step reaction and $GPCeO_2$ and GPCeZr syntheses are one step. The nanoparticle colloids serve to enhance mechanical properties and also provide unique optical properties such as absorbing UV irradiation. In preparation, a minute amount of catalyst is employed to produce a sol which is stable for several months and can easily be polymerized by low temperature curing to produce transparent, dense, hard and abrasion resistant materials.

3.2 Experimental

3.2.1 Synthesis of $GPSiO_2$:

Materials:

- Ludox® TMA Colloidal Silica, Grace Davison, used as received
- 3-Glycidoxypropltrimethoxysilane (GPTMS), ACROS Organics, used as received
- Aluminum Perchlorate $Al(ClO_4)_3$ Nonahydrate 99%, ACROS Organics, 10 wt% in H_2O
- BYK-333, BYK-Chemie, 1 wt% in H_2O
- Zonyl FSO-100 fluorosurfactant, Aldrich, 1 wt% in H_2O
- Isopropyl Alcohol 70%, ACROS Organics, used as received
- Deionized Water

In a typical synthesis, 22.88 g GPTMS and 34.23 g TMA were combined and stirred for 5 minutes. 1.86 g $Al(ClO_4)_3$•$9H_2O$ (10 wt% in H_2O) and 2.86 g BYK-333 (1 wt% in H_2O) were then added to solution and mixed for 1h 45min. Finally, 1.86 g FSO (1 wt% in H_2O), 7.63 g Isopropyl Alcohol and 28.60 g deionized water were added and solution was stirred for an additional 5 min.

3.2.2 Synthesis of GPCeZr:

Materials:

- Cerium Oxide 20% colloidal in H_2O, Alfa Aesar, used as received
- Zirconium Oxide 20% colloidal in H_2O, Alfa Aesar, used as received
- 3-Glycidoxypropltrimethoxysilane (GPTMS), ACROS Organics, used as received
- Aluminum Perchlorate Nonahydrate 99%, ACROS Organics, 1 wt% in H_2O
- Zonyl FSO-100 fluorosurfactant , Aldrich, 1 wt% in H_2O
- Deionized water

32.67 g Cerium Oxide, 32.7 g Zirconium Oxide, 26.0 g GPTMS, 4.6 g $Al(ClO_4)_3$•$9H_2O$ (1% in H_2O) and 3.9 g FSO (1 wt% in H_2O) were combined and stirred for 10 min. The solution was then diluted 5:3 with H_2O.

3.2.3 Synthesis of $GPCeO_2$:

Materials for $GPCeO_2$ are identical to GPCeZr, excluding ZrO_2.

65.6 g Cerium Oxide, 26.0 g GPTMS, 4.6 g $Al(ClO_4)_3 \cdot 9H_2O$ (1% in H_2O) and 3.9 g FSO (1 wt% in H_2O) were combined and stirred for 10 min.

All solutions were dip coated on substrates for characterization. Substrates were prepared by cleaning with water, dilute HCl and ethanol. After coatings, films were dried for 2 hours in ambient conditions and cured at 120°C.

3.2.4 Characterization:

Microhardness, adhesion and abrasion resistance tests were used to characterize the mechanical properties of the materials. Microhardness tests were performed on aluminum 6061 substrates using a Micromet microhardness tester, with a Vickers indenter. At least 10 microhardness indentations were made on each coating. Adhesion was performed on Al 6061 substrate using Gardco Paint Adhesion Test Kit. Samples were prepared as outlined in ASTM D 3359, Test Method B – Cross-Cut Tape Test. At least 5 cross-cut tape tests were performed on each coating.

Abrasion tests were performed on polycarbonate plates using a rotary Taber Abrader with a 250 g load. Following abrasion, a Shimadzu UV-2101PC UV-Vis Spectrophotometer (420 nm) was used to determine the percent transmittance in the wear track area. The wear area was also directly observed using a Hitachi S-3200N Scanning Electron Microscope (SEM). The coatings were applied to polycarbonate, dried for 2 hours followed by curing for 24 hours at 90°C. Lower curing temperature was used in preparing these samples due to thermal properties of polycarbonate.

Fourier transform infrared (FTIR) spectroscopy of coating samples were obtained by Attenuated Total Reflectance (ATR) from 4000-650 cm^{-1} using a Nexus 470 FTIR with Avatar OMNI Sampler using a Ge crystal. X-Ray Diffraction (XRD) analysis was performed on cured films on silica glass microscope slides using a Rigaku D/Max-B X-ray diffractometer (nickel filtered Cu Kα radiation (λ=1.54056 Angstrom) under 35 kV and 30 mA). Philips CM12 electron microscope operating at 100 kV accelerating voltage was used for transmission electron microscopy (TEM) imaging. TEM copper grids (400 mesh) coated with amorphous formvar-carbon film were purchased from SPI Supplies. TEM films were prepared by dip coating the copper grids followed by 12 hr UV curing under 254 nm UV lamp.

UV absorbance due to metal oxide nanoparticles was proven using UV-2101PC UV-Vis Spectrophotometer on scanning mode from 800 to 200 nm.

3.3 Results and Discussion

The coating sols contain FSO-100, a water-soluble ethoxylated nonionic fluorosurfactant that gives exceptionally low aqueous surface tensions. It also improves antisoiling, antifogging and UV resistance in coatings[62]. All coatings also contain 3-Glycidoxypropltrimethoxysilane (GPTMS). GPTMS contains an epoxide ring that can be opened to form polyethylene oxide chains, which enhances the mechanical properties such as elasticity and lowers the thermal densification temperature of the films (relative to purely inorganic materials). We employ aluminum perchlorate as a catalyst, which has been previously demonstrated as a highly effective catalyst for GPTMS organic polymerization (Chapter 2). The acid catalyzes the epoxy ring while at the same time

initiates inorganic hydrolysis and subsequent condensation. Further curing locks in the nanocomposite Si-O-Si/C-O-C network.

$GPSiO_2$ contains Ludox® TMA aqueous colloidal silica, composed of mono-disperse silica particles (~20 nm). During drying, hydroxyl groups on the surface of the particles condense by splitting out water to form siloxane bonds. The particles also develop strong adhesive and cohesive bonds and serve as effective binders in coatings[63]. $GPSiO_2$ also contains BYK-333, a silicone surface additive which helps provide good surface wetting and anti-crater performance by reduction of surface tension. BYK-333 is a polyether modified dimethylpolysiloxane copolymer, containing no solvent[64]. There is no chemical interaction between GPTMS and BYK, the surface additive only provides enhanced physical properties. $GPSiO_2$ synthesis is a two-part reaction. Acid catalyst is added and the solution is allowed to stir while hydrolysis and epoxy ring open initiate. After adequate time, surfactant and solvents are added to the solution to form a stable, pre-reacted sol which is ready for coating and has a shelf life of up to one year. Unlike the other two coatings, in $GPSiO_2$ silica nanoparticles chemically link with the network through Si-O-Si and Si-O-C bonds.

GPCeZr and $GPCeO_2$ are very similar, differing only in concentration and incorporation of metal oxide nanoparticles. GPCeZr contains cerium oxide and zirconium oxide nanoparticles; $GPCeO_2$ contains only cerium oxide colloid and is more concentrated than GPCeZr (lower water content). These solutions are synthesized through "one-pot" synthesis in which all the chemicals are combined simultaneously and a stable homogeneous sol is formed in only 10 minutes. The metal oxide nanoparticles are distributed throughout the network in coatings prepared from these sols.

Average Vickers hardness, standard deviations and converted hardness values are shown in Tables 3.3.1 (2 hour curing) and 3.3.2 (24 hour curing). Adhesion results are shown in Table 3.3.1.

Table 3.3.1: Microhardness and Adhesion (cured 2 hr at 120°C)

Coating	Vickers Hardness (kgf/mm^2)	Std. Dev.	Converted Hardness (Gpa)	Adhesion
$GPSiO_2$	45.43	2.32	0.445	4B
GPCeZr	143.93	8.58	1.411	5B
$GPCeO_2$	96.38	6.39	0.945	5B

Table 3.3.2: Microhardness Results (cured 24 hr at 120°C)

Coating	Vickers Hardness (kgf/mm^2)	Std. Dev.	Converted Hardness (Gpa)
$GPSiO_2$	60.85	3.45	0.597
GPCeZr	145.38	0.57	1.426
$GPCeO_2$	140.53	4.41	1.378

Table 3.3.3: Microhardness of films vs. conventional polymers and other hybrid coatings

Material		Vickers Hardness (GPa)
Polyethylenetherephtalate (PET)		0.23
Polymethylmethacrylate (PMMA)		0.19
Polycarbonate (PC)		0.14-0.16
Hard ormosil (Hybrid sol-gel)		
Polydimethylsiloxane 3% wt-SiO_2		1.57
Polydimethylsiloxane 10% wt-SiO_2		0.86
SiO_2-TiO_2 (Hybrid sol-gel)		1.04
Our materials (Hybrid sol-gel)		
$GPSiO_2$		**0.60**
GPCeZr		**1.43**
$GPCeO_2$		**1.38**

The adhesion was very good for all coatings, especially GPCeZr and $GPCeO_2$. For $GPSiO_2$, the adhesion was rated class 4B, indicating that small flakes of the coating are detached at intersection with less than 5% of lattice patterns. For both GPCeZr and $GPCeO_2$ the adhesion was rated 5B, indicating 0% removal of the coating. The hardness of GPTMS based coatings increases with increase in thermal curing time[65]; comparing

Table 3.3.1 and 3.3.2 shows a clear increase in the microhardness of all coatings (2 hr vs 24 hr curing at 120°C). Furthermore, the hardness of these three water-based films is quite high when compared with conventional plastics such as polycarbonate or polymethylmethacrylate (Table 3.3.3). The materials developed in this research also compare well with other sol-gel hybrid materials including those reinforced with silica particles. In fact, GPCeZr and GPCeO_2 employ no direct organic solvent and nearly achieve the hardness of hard PDMS-SiO_2 *ORMOSILS*. Although it should be noted that other, more advanced sol-gel derived materials exist which exhibit much higher hardness values (up to 35 GPa). However these materials typically require complicated deposition procedures, more advanced synthesis conditions and often unique precursors.

Abrasion resistance is often be characterized by using a transparent substrate such as polycarbonate and abrading the surface with a specified load and number of cycles. Light transmittance as a function of wear cycles can then be compared between the coated and uncoated substrates. Figure 3.3.1 shows percent transmittance in the wear track as a function of wear cycles for uncoated polycarbonate and the three coatings obtained after 24 hour curing at 90ºC.

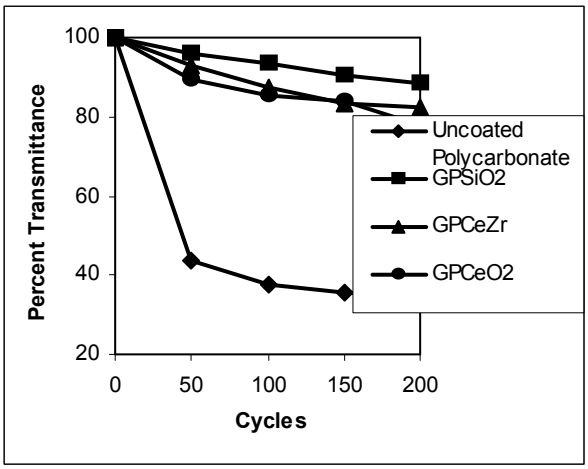

Fig. 3.3.1 Light Transmittance in wear track as a function of wear cycles. All coatings show very high light transmission after abrasion compared with uncoated polycarbonate. Coating 1 shows highest light transmission, therefore highest abrasion resistance.

From Figure 3.3.1, it is clear that all coatings show very high abrasion resistance relative to polycarbonate with $GPSiO_2$ films having the highest abrasion resistance. Although $GPSiO_2$ has the lowest hardness value, it is apparent that BYK-333 additive and Ludox® TMA significantly enhance the abrasion resistance. GPCeZr and $GPCeO_2$ show very high abrasion resistance as well and even after 200 cycles under 250 g load, they still show approximately 80% light transmittance in the wear track. Figure 3.3.2 shows SEM images of the coatings after 250 wear cycles under 250 g load. A very rough surface after abrasion indicates poor abrasion resistance; a smooth surface indicates high abrasion resistance. The images show that polycarbonate is very rough after abrasion, whereas the coatings are still fairly smooth and the wear mechanism can be clearly observed. This confirms the undoubted abrasion resistance improvements relative to polycarbonate.

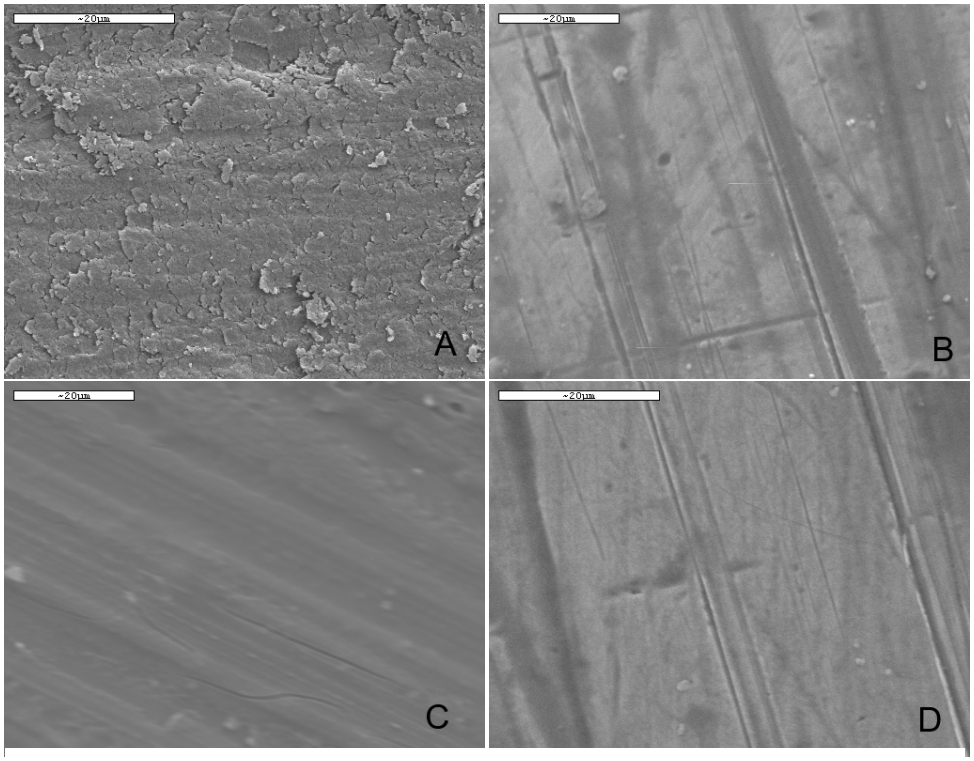

Fig. 3.3.2 SEM micrographs (scale bar 20 microns) of wear area after abrasion cycling. A) Uncoated Polycarbonate, B) $GPSiO_2$, C) GPCeZr, (D) $GPCeO_2$. Clearly all coatings show much smoother surface than uncoated polycarbonate after abrasion cycling.

Fourier Transform Infrared Spectroscopy (FTIR) was performed before and after curing to investigate film structures and verify the formation of the organic/inorganic network. FTIR spectra of $GPSiO_2$, GPCeZr and $GPCeO_2$ films are shown in Figures 3.3.3, 3.3.4 and 3.3.5, respectively.

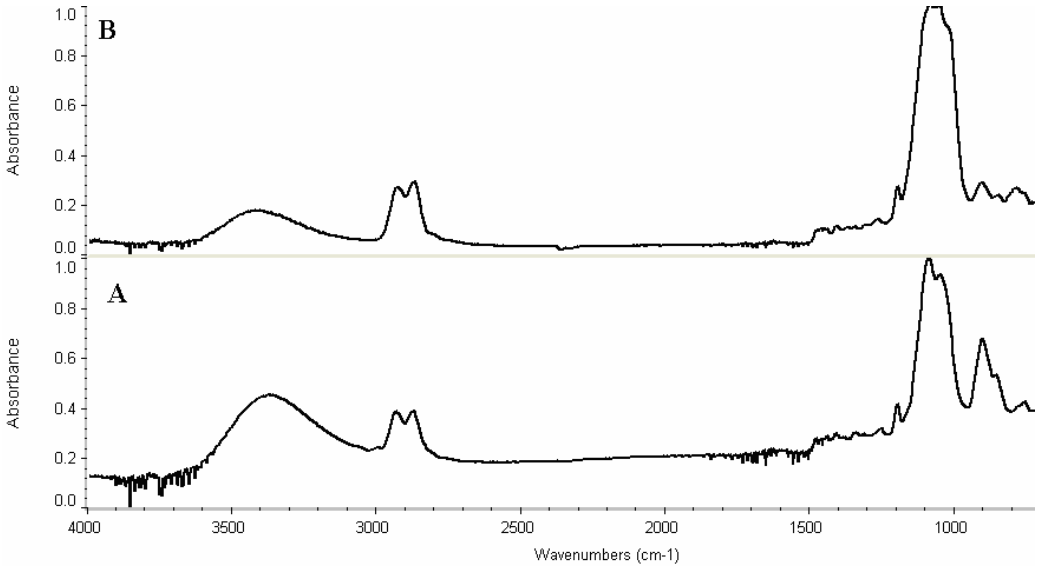

Fig. 3.3.3 FTIR spectra of $GPSiO_2$ (A) after drying, (B) after 2 hour curing at 120°C

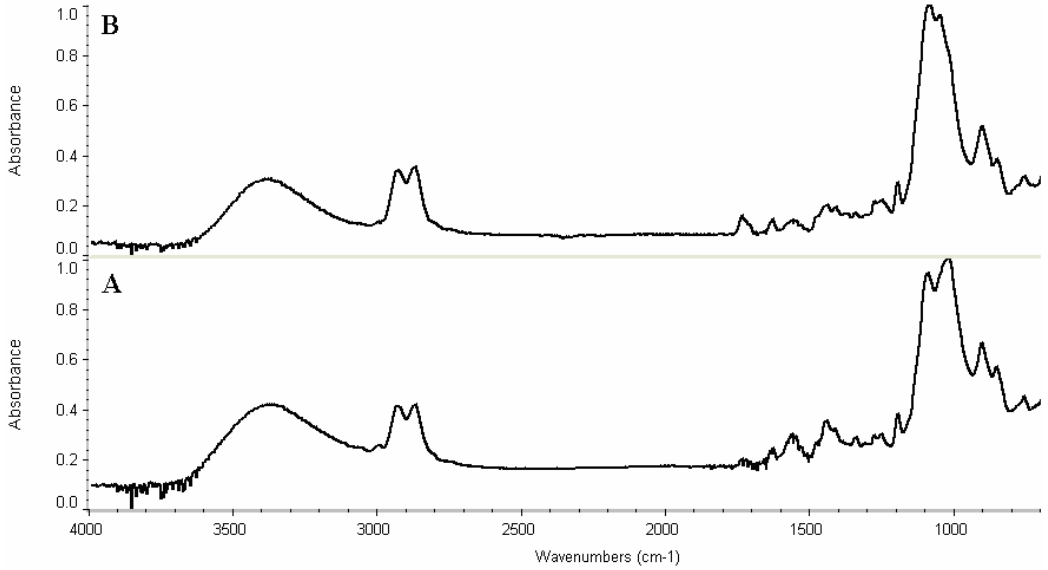

Fig. 3.3.4. FTIR spectra of GPCeZr (A) after drying, (B) after 2 hour curing at 120°C

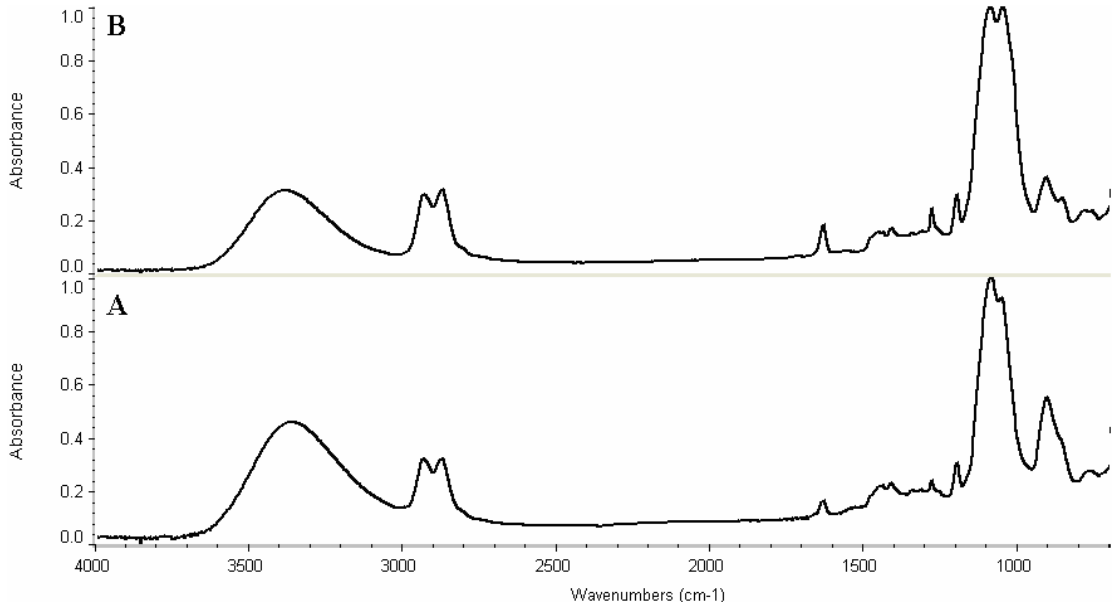

Fig. 3.3.5 FTIR spectra of $GPCeO_2$ (A) after drying, (B) after 2 hour cure at 120°C

GPTMS epoxy rings show characteristic IR absorption bands at 1251-1241 (ring breathing), 912-920 (asymmetric ring deformation), and 840-853 (symmetric ring deformation) cm^{-1}. The C-H stretch in the epoxy also gives rise to another absorption band at 3065-3038 cm^{-1}. IR spectrum of GPTMS shows epoxy bands peaking at 3050, 1254 and 855 cm^{-1}, which were used as a reference to monitor epoxy ring opening by $Al(ClO_4)_3$.

The peaks around 1220 and 1090 cm^{-1} are associated with Si-O-Si/C-O-C asymmetric bond stretching vibration were present in all samples. Peaks around 750-800 cm^{-1} associated with Si-O-Si symmetric bond vibration were also observed in all samples. The broad bands centered near 3400 cm^{-1} are assigned to residual Si-OH stretching vibrations and hydrogen-bonded water. Signals at 910 cm^{-1} arise due to both epoxy groups and Si-OH or $Si\text{-}O^-$ groups. All dried samples show weak residual epoxy signals at 855, 1250 and 3050 cm^{-1}.

After 2 hr curing at 120ºC (Fig 3.3.3B), $GPSiO_2$ shows no residual epoxy groups and a highly cross-linked organic/inorganic network has formed as shown by the strong broad signal ~1090 cm^{-1}. GPCeZr and $GPCeO_2$ show very weak epoxy bands at 855 cm^{-1} after curing, but show no epoxy bands at 1250 cm^{-1} or 3050 cm^{-1}, indicating most epoxies have polymerized. $GPSiO_2$ shows complete organic polymerization after 2 hr curing due to slightly higher catalyst concentration and incorporation of colloidal silica, which we have shown to expedite GPTMS cross-linking. Nanoparticles in all the materials serve as nucleation sites which promote polymer precipitation, allowing for very little catalyst use during synthesis. However, silica particles demonstrate a secondary catalytic effect due to surface silanols, which contribute to epoxy ring opening.

The absorption band around 820 cm^{-1} in GPTMS, which is due to Si-O(CH_3) symmetric stretching vibration, has vanished in all samples indicated inorganic hydrolysis has occurred. Hydrolysis is further confirmed by the change in the GTPMS absorption bands at 2940 and 2840 cm^{-1} which are attributed to C-H asymmetric and symmetric stretching in Si-O-CH_3 respectively. As with $GPSiO_2$, GPCeZr and $GPCeO_2$ show formation of organic/inorganic networks with strong broad Si-O-Si/C-O-C bands around 1090 cm^{-1} and 1200 cm^{-1}. Si-O-Si stretching vibrations in linear and less cross-linked structures give rise to bands around 1120 and 1160 cm^{-1}, which are not observed in any of the films, indicated highly cross-linked cyclic structures.

Figure 3.3.6 shows XRD patterns of coatings obtained after 12 hours curing at 120ºC. All films are amorphous; the patterns for GPCeZr and $GPCeO_2$ are in good accord with those of pure ZrO_2 and CeO_2. The TEM micrograph of $GPSiO_2$ in Figure 3.3.7A clearly shows a worm-like amorphous network with silica particles

homogeneously dispersed throughout. Non-ionic (NI^0) surfactant pathways lead to amorphous worm-like structures as seen in the figure. 3.3.7B and 3.3.7C show images of GPCeZr and $GPCeO_2$ respectively. The particle reinforcement in these materials is not mono-disperse as in $GPSiO_2$ so resulting films have some particle agglomeration during synthesis and drying. Regardless, the amorphous, porous, worm-like structure results and mechanical and optical performance remains.

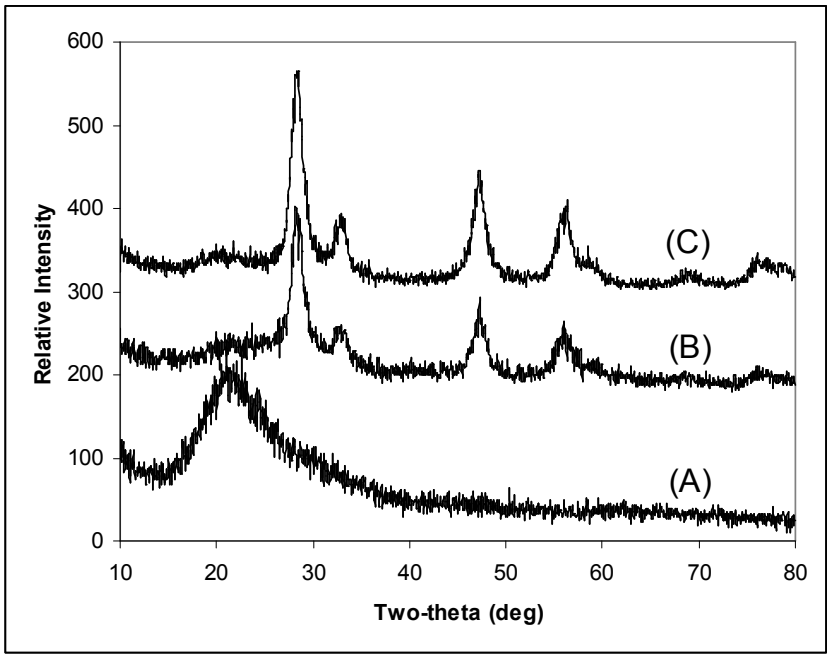

Fig 3.3.6 X-ray diffraction patterns of (A) $GPSiO_2$, (B) GPCeZr, and (C) $GPCeO_2$ after 12 hour curing at 120ºC. XRD pattern of $GPSiO_2$ confirms amorphous structure, patterns of GPCeZr and $GPCeO_2$ are in accord with XRD patterns of pure CeO_2 and ZrO_2.

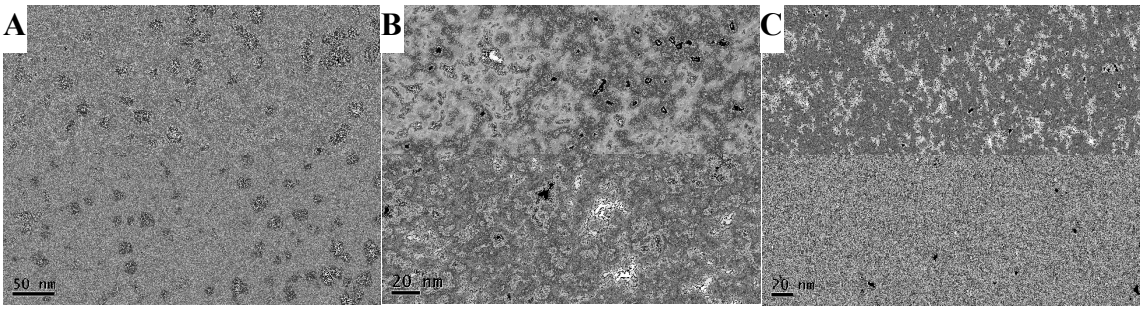

Fig 3.3.7 Transmission electron microscope images of (A) $GPSiO_2$, (B) GPCeZr and (C) $GPCeO_2$ after 12 hour UV curing

Figure 3.3.8 shows UV absorption of the coating sols. From the figure, $GPSiO_2$ shows little UV absorbance, although there is a small amount of UV-absorbance on the lower end of the spectrum (around 200 nm) which is likely due organic/inorganic sol particulate absorption. However GPCeZr and $GPCeO_2$ show strong absorbance of UV waves, especially from 200 to 300 nm, which are very harmful to humans. This UV absorption is due to the incorporation of metal oxide nanoparticles. $GPCeO_2$ shows much stronger absorption due to its higher concentrations (GPCeZr is diluted 5:3 with H_2O). When large particles are used as additives in polymers, scattered UV light concentrates

near the particles, which can cause photodegradation in the region around the particles. The intensity of the light scattered from a particle is governed by the Mie Equation, and therefore as the particle size approaches the nanoscale, the particles effectively absorb UV radiation rather than scatter it[66]. The particles employed in this experiment are 5 – 20 nm in diameter, therefore are extremely effective in absorbing UV light. The metal oxide nanoparticles also absorb 300-400 nm UV irradiation, which can reach the earth's surface and cause skin disease. Thus GPCeZr and $GPCeO_2$ have important applications in protecting humans or other material sensitive to UV irradiation[67].

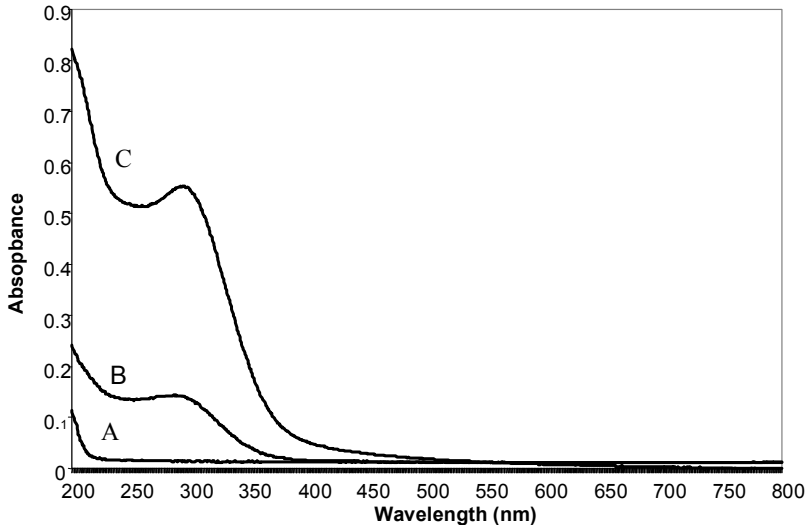

Fig. 3.3.8 Absorption spectroscopy of coating sols diluted 10,000 times in H_2O. (A) $GPSiO_2$, (B) GPCeZr, (C) $GPCeO_2$

3.4 Summary

We have synthesized three novel organic-inorganic water-based nanocomposite coatings, which are relatively hard and abrasion resistant with very good adhesion. . Two of the coatings are useful for protecting humans or other UV sensitive materials from harmful UV irradiation. Incorporation of nanoparticle colloids allows minimal catalyst use and provides facile and green synthesis of coating sols which have long shelf life. Short curing at low temperature concludes polymerization to produce dense, hard films. All coatings have unique properties and can serve numerous applications, especially as protective and multi-functional coatings. The synthesis and application of all coatings is simple, fast and produces very few harmful byproducts, making them ideal materials in industry.

Chapter 4. Enhancing Mechanical Properties of Silica Aerogels Through Nanoengineering

4.1 Introduction

Practical application of aerogel materials has been slow because aerogels are brittle and hygroscopic. Due to their extraordinary porosity, aerogel materials rapidly absorb moisture from the environment, which leads to structural collapse due to the capillary forces that develop in the pores. Improving the poor mechanical properties of silica aerogels has been a topic of study for the past decade. We have developed a novel method to prepare modified silica aerogels, in which a small amount of Laponite® RDS, a water-soluble inorganic synthetic nanocomposite is added. The molecular-level synergism between silica nanoparticles and molecular cross-linkers inverts the relative host-guest roles in glass-polymer composites, leading to more robust low-density materials.

4.2 Experimental Section

4.2.1 Gel Synthesis

Pure silica aerogels without Laponite® were prepared using a two-step acid-base catalysis method. In order to minimize the aerogel's density while maintaining uniform pore and particle sizes, the molar ratio of tetraethyl orthosilicate (TEOS) to ethanol (EtOH) to water (H_2O) was TEOS:EtOH:H_2O = 1:5:7[23]. TEOS, EtOH and water were

combined in a glass beaker under magnetic stir. Hydrolysis was induced by adding 1 N hydrochloric acid (HCl) dropwise until the pH of the solution was between 2 and 2.6[68]. The solution was then covered and stirred for 1 hour under ambient conditions. 1 N ammonium fluoride was then added dropwise to raise the pH of the solution to ~5 for gelation. The sol was quickly poured into cylindrical polystyrene molds before gelation. The gels were aged in their molds for forty-eight hours and then placed in pure EtOH to remove residual water and unreacted precursors. The gels were aged in the EtOH bath for three days and fresh ethanol was exchanged at least 3 times before drying.

For nanocomposite aerogel samples containing Laponite® RDS, the percentage of the Laponite® added was relative to the weight of TEOS. The molar ratio of TEOS:EtOH:H_2O was 1:5:7. In a typical synthesis, 60 mL of TEOS (ρ = 0.94 g/mL) was used, which weighs 56.4 g. Thus for 1% Laponite® addition, 0.56 g of Laponite® RDS was mixed with water to form a Laponite® dispersion. Laponite® was added to water to create a dispersion: 1% used 10 mL, 2.5% used 25 mL, 5% used 50 mL and 7.5% used 75 mL H_2O. The Laponite® and water were rapidly stirred for 30 minutes prior to mixing with TEOS and EtOH to ensure complete Laponite® dispersion and hydration.

4.2.2 Supercritical drying

The gels were dried using supercritical carbon dioxide (CO_2) solvent exchange. The drying apparatus is shown in Figure 4.2.1. An ISCO 500D series syringe pump with computer controller was used to supply liquid CO_2 to the system. Temperature was controlled using K-type thermocouples, temperature controllers (Omega CN132 and CN800 Series) and heating tape. A CO_2 pre-heating cylinder was used between the CO_2 pump and the autoclave to heat the CO_2 to 40ºC before mixing with ethanol in the cell.

This helps to prevent capillary forces (due to liquid-vapor interfaces) on the gel pores and avoid gel cracking.

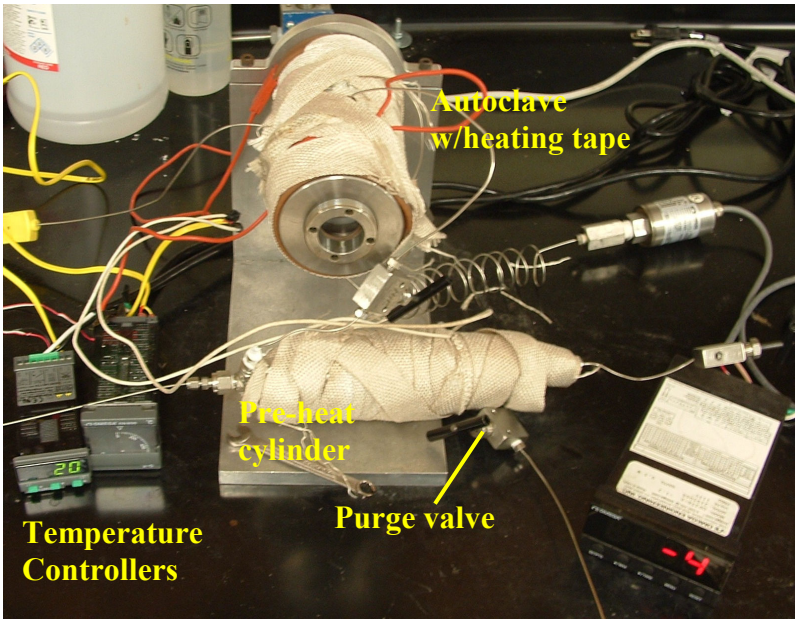

Figure 4.2.1 Supercritical drying apparatus

First the samples were submerged in EtOH within a 100 mL stainless steel autoclave. The gels were situated upon thin steel rods to ensure maximum solvent-gel contact and improve ethanol/CO_2 diffusion. The cell was heated to 40ºC at +5ºC/min. The cell was then pressurized to 1400 psig at +20 psi/min. CO_2 is supercritical at 1070 psi and 31.1^{o}C CO_2, so 1400 psi and 40^{o}C ensure that the CO_2 is supercritical. The cell was then flushed with CO_2 at ~7 mL/min flowrate (~1.14 g/min at 1400 psig) at constant pressure to remove ethanol from the cell and exchange solvent in the gels. Typically about 700 mL CO_2 (1400 psig), which is seven times the cell volume was required to dry the gels. After removing all possible residual EtOH from the gels, the cell was depressurized at -3 psi/min to atmospheric pressure at a constant 40^{o}C.

4.2.3 Characterization

Thermal conductivity of the aerogel samples was measured via the parallel hot wire method. The cylindrical sample was split into two semi cylindrical halves and then two small parallel trenches were cut into one of the halves at a distance of about 1 mm apart. The hot wire and thermocouple were covered with aerogel powder to ensure adequate contact and then compressed between the two halves so that each wire fit into one of the parallel trenches (see Figure 4.2.2). The thermocouple was a type-S Pt/Pt-10%Rh with a diameter of 0.003 mm. Thermocouple leads were connected to copper wires which were connected to a National Instruments Data Acquisition Board. The thermocouple ends were placed in ice baths to negate the thermocouple-wire junctions. Heating profiles were obtained using Labview. The hotwire was a platinum wire with a 0.003 mm diameter.

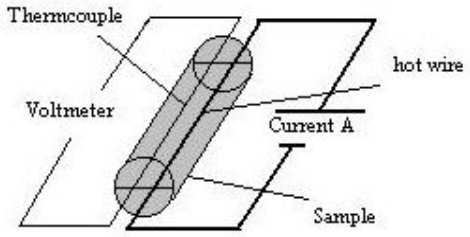

Figure 4.2.2 Parallel hotwire setup for thermal conductivity

Mechanical strength of the aerogels was measured using 3-point bending method. An Instron model 4411 desktop Universal Material Test system with a custom 500 N load cell was used for all tests. The length L of the supports was 30 mm and the force F and deflection were measured by the load and strain transducers, respectively. A schematic of the 3-point bending setup is shown in Figure 4.2.3.

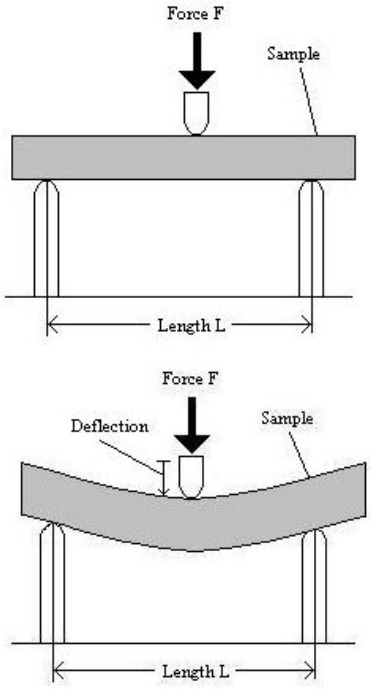

Figure 4.2.3 3-point bending setup

Brunauer, Emmett and Teller (BET) method was employed to measure aerogel surface area, pore volume, porosity and pore size distributions.

4.3 Results

The hot wire method is a transient dynamic technique. The process was to apply a current across the hot wire for a set amount of time and then measure the change in voltage of the thermocouple. The change in temperature of the thermocouple can then be derived from the change in voltage[69]. Labview provided direct translation to thermocouple temperature readings. The thermal conductivity of the aerogel sample is then calculated using the temperature change with respect to time:

$$\theta - \theta_0 = \left(\frac{q}{4\pi\lambda}\right)\left[-0.5772 + \ln\left(\frac{4at}{r^2}\right)\right]$$

where θ is the temperature of the thermocouple, θ_0 is the temperature prior to heating, q is the power dissipated per meter of the hot wire, r is the radius of the hotwire, λ is the thermal conductivity, and a is the thermal diffusivity of the medium surrounding the

wire[70]. The equation above is valid for large times, or rather for $at/r^2 >> 1$. If the temperature rise is sufficiently small for λ and a to remain constant, θ will be linear with respect to ln t, with the slope being $\frac{d\theta}{d(\ln t)} = \frac{q}{4\pi\lambda}$. Therefore, with certain conditions, the thermal conductivity λ can be determined directly from the temperature variation θ(t). In our experiments, the temperature rise was sufficient small (only a few degrees) over a relatively long period of time (30-60 seconds) and the radius of the hotwire is quite small (0.0015 mm), so $at/r^2 >> 1$ and the second equation holds valid. An example of the temperature profile (in log scale) of a pure silica aerogel is shown in Figure 4.3.1. The linear region can clearly be observed over a 30 second period.

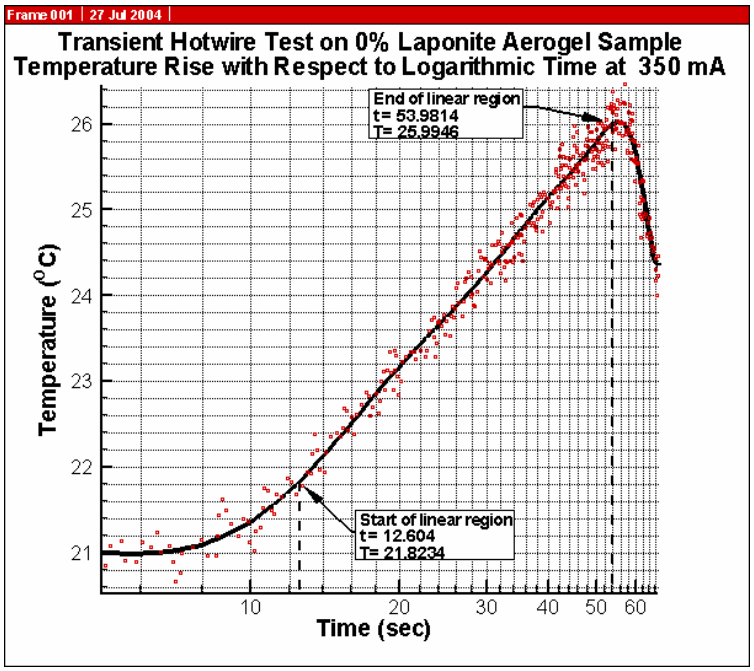

Figure 4.3.1 Temperature vs. ln(t) of pure silica aerogel from transient hotwire method

Mechanical properties from 3-point bending, bulk density measurements and thermal conductivity measurements are shown in Table 4.3.1. The modulus of elasticity

E was measured using the relation $E = \frac{SL^3}{12\pi r^4}$, where S is the slope of the stress-strain curve, L is the span of the two supports, and r is the radius of the sample[71].

The results show that the yield strength increases up to 2.5% Laponite®. At 2.5% loading, the nanocomposite has twice the yield strength of the pure silica aerogel. Despite the significant strength increase, the stiffness of the 2.5% gels is roughly 3X higher than that of the pure silica aerogels and the density is also increased. At 1.0% Laponite® RDS, mechanical strength increases 22% while the modulus of elasticity decreases 25% and density is lowered slightly. At 5.0% Laponite® addition, both the strength and density of the pure aerogel is maintained, but the modulus of elasticity is lowered ~21%. At higher Laponite® loading of 7.5%, the gel is significantly weakened (47.5% decrease in strength), however the modulus of elasticity is lowered 59.5%. Lowering the elastic modulus of silica aerogels while retaining the density and thermal conductivity, is a significant achievement. Pure silica aerogels are extremely brittle and fracture very easily. Increasing the elasticity of the gels allows access to new applications where previous aerogel materials were unacceptable. For the 1% and 2.5% samples, the increased strength of the gel networks also helps prevent pore collapse on contact with moist air. It is apparent that relatively low concentrations of Laponite® RDS (i.e. 1%) are more suitable for improving the mechanical properties of silica aerogels. Higher loading leads to more elastic gels, but with sacrifice of strength. It is desired to increase the strength, while decreasing the modulus of elasticity.

Table 4.3.1 Mechanical properties of aerogel samples

% Laponite	Yield Force (N)	Yield Strength (kPa)	Modulus (Mpa)	Bulk Density (g/cm^3)	Thermal Conducitivity (W/mK)	Surface Area (m^2/g)	Pore size (nm)
0.0%	1.8	162.6+/-33.4	6.10+/-1.68	0.1780	0.021		
1.0%	1.3	198.7+/-15.4	4.53+/-0.29	0.1664	0.025	1177	6.08
2.5%	1.8	316.6+/-6.6	18.35+/-4.88	0.2019	0.027		
5.0%	1.3	160.7+/-24.4	4.80+/-1.40	0.1785	0.027	808	12.05
7.5%	0.7	85.3+/-16.4	2.47+/-0.53	0.1536	0.024	860	18.5

Furthermore, the nanocomposite samples retain the remarkably low thermal conductivity of pure silica aerogel. In aerogels, the thermal conductivity is dependent on collisions between gas molecules in the pores, conduction through the solid skeleton, and radiation. Although Laponite® is a crystalline ceramic material, and has slightly higher thermal conductivity than silica aerogels, the crystallites are dispersed throughout the aerogel networks and align in a manner so that thermal conduction is inhibited. Preliminary BET results (not shown) show that the pore size and pore size distribution is not greatly altered by the addition of Laponite®. In all samples analyzed by BET, the surface area remains greater than 800 m^2/g and the average pore size remains below 20 nm. Thus gas diffusion within the pores should be comparable. Radiation heat transfer is unaffected by Laponite® addition.

4.4 Discussion

Laponite® RDS is a sol forming grade of synthetic layered crystalline silicate incorporating an inorganic polyphosphate peptiser. Its composition is 54.5% SiO_2, 26.0% MgO, 0.8% Li_2O, 5.6% Na_2O and 4.4% P_2O_5. When added to water, Laponite® RDS hydrates and swells to give colorless, translucent, low viscosity colloidal dispersions. The nanoscale Laponite® crystals can be understood as two-dimensional polymeric discs with negatively charged surfaces and positively charged edges as shown in Figure 4.4.1[72].

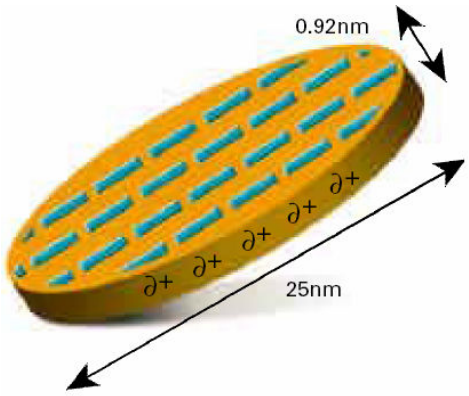

Figure 4.4.1 Laponite particle structure

Laponite® RDS contains a small amount of tetrasodium phosphate (TSPP). When added to water, the blended TSPP dissolves and pyrophosphate $(P_2O_7)^{4-}$ anions become associated with the positively charged edges of the crystal (Figure 4.4.2), thereby imparting an overall negative charge to the particle. The negative charge of the crystal causes it to be surrounded by a layer of hydrated sodium ions, whose positive charges cause the crystals to repulse one another. When hydrated, electrostatic attractions draw the sodium ions in solution toward the crystal surface and osmotic pressure from the water pulls them away, and equilibrium is reached. The sodium ions are held in a diffuse region on both sides of the dispersed Laponite crystal, known as electrical double layers. Thus when two particles approach their mutual positive charges repel each other and the particles remain dispersed in solution.

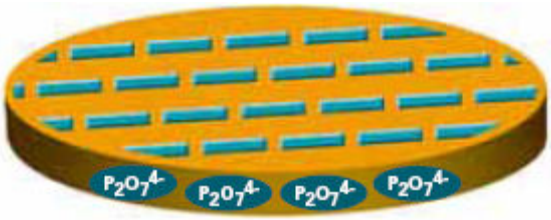

Figure 4.4.2 Individual Laponite particle stabilized by peptiser

Upon addition of TEOS and EtOH to the Laponite® dispersion, the dispersing effect of the TSPP is overcome as the pyrophosphate anions are absorbed by the solution and newly forming silica condensates. As this happens, the adjacent Laponite® crystals will begin to interact with each other and the "house of cards" structure (Figure 4.4.3) can form, which results in viscosity increase. Indeed the viscosity of the precursor solution was seen to increase significantly (over pure aerogel solutions) when the Laponite® dispersion was mixed with TEOS and EtOH.

Figure 4.4.3 Laponite "house of cards" structure

We theorize that Laponite® crystal interactions are initiated upon mixing the dispersion with TEOS and EtOH although most of the particles retain the electric double layer and remain dispersed during hydrolysis. As the precursor silanols begin to condense, the newly formed silica chains and particles absorb the pyrophosphate anions and the Laponite® crystals stack themselves within the forming silica phases. Furthermore, the Laponite® crystals contain hydroxyl end groups which can condense with silanols to chemically link the crystals with the silica particles. The molecular structure of Laponite® RDS is shown in Figure 4.4.4. The inter-layered tetrahedral and octahedral structures provide a spring-like effect, thereby giving the network greater elasticity and allowing it to withstand higher compressive forces, which gives the bulk nanocomposite samples higher mechanical strength (at 1% and 2.5% addition). When the

concentration of the Laponite® dispersion increases, the "house of cards" structure has a more dominating effect and the spring-like structure of the Laponite® crystals imparts greater elasticity to the gel network. Additionally, the unique molecular structure allows higher structural stability and prevents syneresis or collapse of the tenuous network. This is very important in applications, especially in the presence of water vapor, which will cause pore collapse. The added structural stability of the Laponite® crystals can also explain the lower density in some of the samples. During aging and drying, the gel network will constrict, resulting in higher density. It is apparent that the Laponite® addition helps prevent the gel shrinkage and maintain even lower density than pure silica aerogels.

We believe the Laponite® crystals interact with the silica network in two ways: firstly the crystals stack and are held in a gel-like "house of cards" structure through electrostatic bonds; secondly, hydroxyl groups on the edges of the crystals bond with newly formed silica aggregates. Thus an interwoven porous stacking structure of Laponite® and silica is achieved. The structures have yet to be investigated by high resolution transmission electron microscopy (TEM) which should help reveal the true nanostructure.

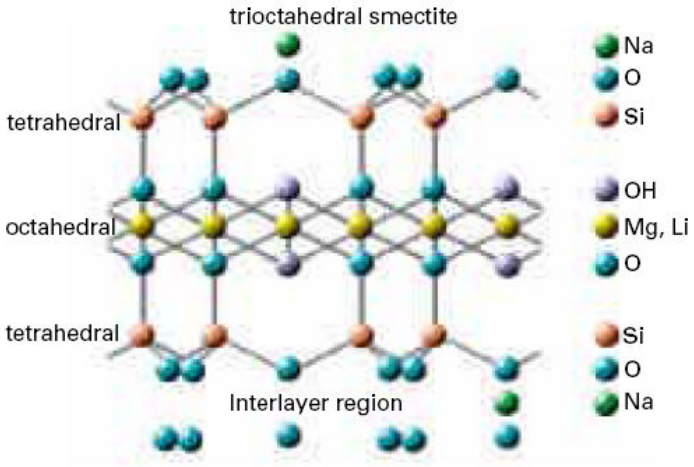

Figure 4.4.4 Laponite molecular structure

As the concentration of the Laponite® dispersion is increased, the crystals are forced into closer contact and more particle-particle interactions between positively charged edges and negatively charged faces will occur. This reduces the mobility of the particles within the dispersion resulting in an increase in viscosity. It is believed that this is the cause for the lower mechanical strength at the higher concentrations of Laponite®. We believe that with the higher concentration samples, the crystal interactions begin before silica sol formation and a Laponite® "house of cards" gel-like structure results early in the sol-gel process. Therefore, rather than being well dispersed throughout the silica phase, the "house of cards" structure dominates within the gel structure. This dominating structure throughout the gel network is a reasonable explanation for the low modulus of elasticity in the 7.5% samples. BET investigation of the 7.5% samples reveal that the average pore size is 18.5 nm, which is very close the Laponite® crystal dimension. It is evident that the pore structure is more greatly governed by the Laponite® "house of cards" structure rather than the silica gel structure at these higher concentrations. TEM should elucidate this theory and reveal whether Laponite® aggregates exist within the silica networks. Scanning electron microscopy has been

performed on some of the nanocomposite aerogel samples, however the resolution is too low to provide clear insight to the structures. The Laponite® crystals have a maximum dimension of only 25 nm and are hard to differentiate from the silica network under SEM conditions. Figure 4.4.5 shows an SEM image of 1% Laponite aerogel at 70kX with 100 nm scale bar.

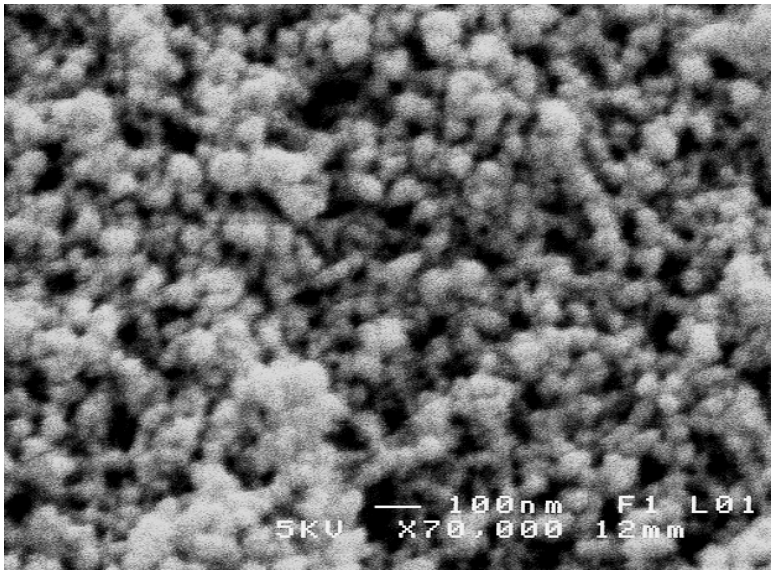

Figure 4.4.5 SEM image of 1% Laponite aerogel with 100 nm scale bar

4.5 Summary

We have developed a synthetic route for fabricating nanocomposite aerogels with enhanced mechanical strength and reduced elastic modulus. Laponite® RDS, a water soluble silicate was incorporated into the sol-gel synthesis of silica aerogels. Laponite® was added at various concentrations to study its effects on network formation and to determine the optimal synthesis conditions. The maximum yield strength was achieved at 2.5% Laponite® (based on TEOS weight), with a twofold increase in strength over pure silica aerogels. 1% Laponite® addition led to an increase in strength and elasticity, with a decrease in bulk density. Higher Laponite® addition (above 2.5%) results in

significantly lower elastic modulus, however with sacrifice of mechanical strength. Furthermore, the extraordinarily low thermal conductivity of silica aerogels is maintained in the nanocomposites. From preliminary BET results, the exceptionally high surface area and porosity of pure silica aerogels is maintained in the nanocomposite samples. More BET experiments are currently being conducted and future work will include high resolution TEM imaging and structural investigation with FTIR.

REFERENCES

[1] Tsakalakos, T.; Ovid'ko, I.A.; Vasudevan, A.K. *Nanostructures: Synthesis,Functional Properties and Applications,* Kluwer Academic Publishers: Dordrecht, Netherlands, **2001**

[2] Goldstein, A.N., *Handbook of Nanophase Materials*, Marcel Dekker Inc., New York, 1997

[3] Hench, L. L. and West, J K. *Chemical Reviews* **1990** 90, 33

[4] Brinker, C.J. and Scherer, G.W., *Sol-Gel Science, The Physics and Chemistry of Sol-Gel Science*, Academic Press, New York, 1990

[5] Sakka, S. *Amercian Ceramic Society Bulletin* **1985** 64, 1463-1466

[6] Johnson, D.W. *American Ceramic Society Bulletin* **1985** 64, 1597-1602

[7] Colomban, Ph. *Ceramics International* **1989** 15, 23-50

[8] Dislich, H. *Journal of Non-Crystalline Solids* **1986** 80, 115-121

[9] Yoldas, B.E. *Journal of Materials Science* **1979** 14, 1843-1849

[10] Kumar, K.N.P; Keizer, K.; Burggraaf, A.J.; Okubo, T.; Nagamoto, H.; Morooka, S. *Nature* **1992** 358, 48

[11] http://www.chemat.com/assets/images/Flowchat72.jpg

[12] http://www.kri-inc.jp/ts/dept/images_e/img_nano-m2_e.gif

[13] (a) Sakka, S. in Better Ceramics Through Chemistry; North-Holland: New York, 1984, p.91

(b) Sakka, S.; Kamiya, K.; Makita, K.; Yamamoto, Y. *J. Non-Cryst. Solids* **1982**, 48, 31

[14] Voronkov, M.G.; Mileshkevich, V.P.; Yuzhelevski, Y.A. *The Siloxane Bond*; Consultants Bureau: New York, 1978

[15] Lin, C.C. and Basil, J.D. in *Better Ceramics Through Chemistry II*, Materials Research Society: Pittsburg, 1986, p. 55

[16] http://www.unifr.ch/physics/mm/proj/coll_solgeltrans.php

[17] Schubert, U.; Husing, N.; Lorenz, A. *Chemistry of Materials* **1995**, 7, 201

[18] Nass, R.; Arpac, E.; Glaubitt, W.; Schmidt, H. *J. Non-Cryst. Solids* **1990,** 121, 370

[19] Amberg-Schwab, S.; Arpac, E.; Glaubitt, W.; Rose, K.; Schottner, G.; Schubert, U. *High Performance Films and Coatings;* Vincenzini, P., Ed.; Elsevier: Amsterdam, 11191; p 203

[20] Kasemann, R.; Schmidt, H. *New J . Chem.* **1994,** 18*,* 1117

[21] Innocenzi, P; Giovanna, B. *Chemistry of Materials* **2000,** 12*,* 3726

[22] Iler, R.K. in *The Chemistry of Silica*; Wiley: New York, 1979

[23] Scherrer, G.W. J. Non-Cryst. Solids **1988**, 100, 77

[24] Wagh, P.B.; Venkateswara Rao, A. *Materials Chemistry and Physics* **1998**, 53, 41

[25] http://www.aist.go.jp/aist_e/research_units/research_section/energy/energy_03.jpg

[26] Pool, R. *Science* **1990**, 247, 807.

[27] Mulder, C.A.M.; Van Licrop, J.G. in: J. Fricke (Ed.), *Aerogels*, Springer: Berlin, **1986**, p. 68

[28] (a) Pajonk, G.M.; Inovna, CR. *Indusrtie et Innovation* (France) **1976** p.376

(b) Pajonk, G.M.; Teichner, S.J. *Aerogels*, in: J. Fricke (Ed.), *Proceedings in Physics*, Springer: **1986**, p. 193

(c) El Tanany, A.; Pajonk, G.M. *React. Kinet. Catal. Lett.* **1992**, 47, 167

(d) Pajonk, G.M. *Appl. Catal*, **1991**, 72, 217

[29] Fricke, J.; Emmerling, A. *Structure and Bonding* 77. Springer: Berlin, **1992**, p. 38

[30] Cooper, D.W. *Part. Sci. Technol.* **1989**, 7, 371

[31] Rasmussen, J.L. Proceedings of the 2nd International Symposium on Aerogcls (Revue de Physique Appliquec. Colloquc (4)). Le, Editions de Physique, Les Ulis Cedex, France, p. 221

[32] Fricke, J.; Arduini-Schuster. M.C.; Burtner., D.; Ebrrt, H.P.; Heinemann, U.; Hetfleisch, J.; Hummer., E.; Kuhn, J.; Lu, X. *2lst International Thermal Cond. Conference*, Lexington. Kentucky, **1989**.

[33] Frickc, J. *Phys. Unsercr Zcit* **1989**, 20, 189

[34] (a) Cantin, M.; Caase., M.; Koch, L.; Jouan, R.; Mcatreau, P.; Roussel, D.; Bonnin, F.; Moutel, J.; Teichner, S.J. *Nucl. Instrum. Methods* **1974**, 118, 177

(b) Bourdinaud., M.; Chezr., J.B.; Tbevenin., J.C. *Nucl. Instrum. Methods* **1976**, 136, 99

(c) Carlson, P.J.; Johansson, K.E.; Kesteman, J.; Norsbay, J.; Pingot, O.; Van Den Bogaert, F.; Van Lanker, L. *Nuci. Instrum. Methods* **1979**, 160, 407

[35] Gonauer, M.; Fricke., J. *Acustica* **1986**, 59, 177

[36] (a) Kim., N.K.; Payne, D.A.; Upadhye, R.S. *J. Vat. Sci. Technol.* **1989**, A7, 181

(b) Jang, K.Y.; Kim, K.; Upadhye, R.S. *J. Vat. Sci. Technol.* **1990**, A8, 1732

(c) Kim, K.; Jang., K.Y.; Upadhye, R.S. *J. Am. Ceram. Soc.* **1991**, 74,1987

[37] Ashley., C.S.; Reed, S.T.; Brinker, C.J.; Walco, R.J.; Ellefson, R.E.; Gill, J.T. in: L.L. Hench, J.K. West (Ed&.), *Chemical Processing of Advanced Materials*, Wiley. New York. **1992**, p. 989

[38] (a) http://www.spaceflightnow.com/news/n0205/08aerogel/aerogel.jpg

(b)http://imglib.lbl.gov/ImgLib/COLLECTIONS/BERKELEY-LAB/RESEARCH-

1991-PRESENT/MATERIALS-SCIENCE/images/96904224.lowres.jpeg

[39] (a) Schmidt, H. *J. Non-Crys.t Solids* **1985**, 73, 681

(b) Brinker, C. J.; Scherer, G. W. *Sol-Gel Science: The Physics and Chemistry of Sol-Gel Processing*; Academic: New York, 1990

(c) Phillip, G; Schmidt, H. *J. Non-Cryst Solids* **1986**, 82, 31

(d) Schmidt, H. *J. Non-Cryst Solids* **1994**, 178, 302

(e) Cassagneau, T.; Caruso, F. *JACS* **2001**, 124, 8172

[40] Popall, M.; Kappel, J.; Pilz., M.; Schulz., J.; Feyder, G. *J. Sol-Gel Sci. Technol*. **1994**, 2, 157

[41] Sorek, Y.; Zevin, M.; Reisfeld, R. *Chem. Mater.* **1996**, 9, 670

[42] Kasemann, R.; Bruck, S.; Schmidt, H. *SPIE* **1994**, *2288*, 321

[43] Epifani, M.; Leo, G.; Lomascolo, M.; Vasanelli, L. *J. Sol-Gel Sci. Technol*. **2003**, 26, 441

[44] Hoebbel, D.; Nacken, M.; Scmidt, H. *J. Sol-Gel Sci. Technol*. **1998**, 12, 169

[45] Templin, M.; Wiesner, U.; Spiess, H.W. *Adv. Mater.* **1997**, 9, 2385

[46] Innocenzi, P.; Brusatin, G.; Guglielmi, M.; Bertani, R. *Chem. Mater.* **1999**, 11, 1672

[47] Shoup, R.D.; *Colloid and Interface Science III*; Academic: New York, 1976

[48] Daniels, M.W.; Francis, L.F. *J. Colloid and Interface Sci.* **1998**, 205, 191

[49] Akitt, J.W.; Duncan, R.H.; Setchell, C. *J. Chem. Soc. Dalton Trans.* **1983**, 2639

[50] Nyquist, R.A. *Interpreting Infrared, Raman, and Nuclear Magnetic Resonance Specta*, Vol 2; Academic: San Diego, 2001

[51] Chmel, A.; Mazurina, E.K.; Shashkin, V.S. *J. Non-Cryst. Solids* **1990**, 122, 285

[52] (a) Viart, N.; Niznansky, D.; Rehspringer, J.L. *J. Sol-Gel Sci. Technol.* **1997**, 8, 183

(b) Voronkov, M.G.; Mileshkevich,V.P.; Yuzhelevskii, Y.A. *The Siloxane Bond*; Consultants Bureau: New York, 1978

[53] Hajji, P.; David, L.; Gerard, J.F.; Pascault, J.P.; Vigier, G. J. *Polymer Sci. B* **1999**, 37, 3172

[54] Almeida, R.M.; Guitton, T.A.; Pantano, C.G. *J. Non-Cryst. Solids* **1990**, 121, 193

[55] Xue, G.; Ishida, H.; Koenig, J.L. *Makromolekulare Chemie* **1986**, 140, 127

[56] Eggersglus, W. *Organische Peroxyde*; Verlag Chemie: Weinheim, 1951

[57] (a) Bayer, E.; Albert, K.; Reiners, J.; Nieder, M. *Journal of Chromatography* **1983**, 264, 197

(b) Liu, Y.; Hsu, C.; Wang, M.; Chen, H. *Nanotechnology* **2003**, 14, 813

[58] Riegel, B.; Kiefer, W.; Hofacker, S.; Schottner, G. *J. Sol-Gel Sci. Technol.* **2002**, 24, 139

[59] Kalinowski, H.O.; Berger, S.; Braun, S. *Carbon 13 NMR Spectroscopy*; John Wiley: Chichester, U.K., 1988, p.181

[60] Kasemann, R.; Schmidt, H. K.; Wintruch, E. *Mater. Res. Soc. Symp. Proc*. **1994**, 346, 915

[61] Mosher, B.P.; Wu, C.; Sun, T.; Zeng, T. *J. Non-Cryst. Solids* **2006**, 352, 3295

[62] Zonyl, Dupont Performance Chemicals, http://www.dupont.com/zonyl

[63] Grace Davison, http://www.gracedavison.com/products/ludox/overview.htm

[64] BYK-Chemie, www.byk-chemie.com

[65] Innocenzi, P. ; Esposto, M. ; Maddalena, A. *Journal of Sol-Gel Sci and Tech.* **2001**, 20 293

[66] Katangur, P. ; Warner, S.; Patra, P.; Kim, Y.; Mhetre, S.; Dhanote, A. "Nano-Structured Polymer Coatings for Ultraviolet Protection," Dept of Textile Science, Univ. Mass. Dartmouth

[67] Li, H. ; Chen, Y. *Journal of Nanoparticle Research* **2001**, 3, 159

[68] M. Stolarski, M.; Walendziewski, J.; Steininger, M.; Pniak, B. *Applied Catalysis A* **1999**, 177, 139

[69] *Revised Thermocouple Reference Tables: Type S Reference Tables N.I.S.T., Monograph 175 Revised to ITS-90.* From Omega Engineering's Temperature Technical Reference Section. p. Z-208.

[70] Sandberg, O.; Anderson, P.; Bäckstrom, G. *Journal of Physics E* **1977**, 10, 474

[71] Gere, J.M.; Timoshenko, S.P. *Mechanics of Materials*, 4th ed.; PWS Publishing: Boston, 1997; pp599-607, 870, 885.

[72] Rockwood Additives, www.laponite.com

Nomenclature

Aerogel – A nanoporous material filled mostly with air, having volume fractions of solid as low as ~1%

Aging – the process of change in gel structure and properties after gelation

Alkoxide – the conjugate base of an alcohol, therefore having an organic group bonded to a negatively charged oxygen atom

Amorphous – non-crystalline

Calcination – heating to a high temperature but below the melting or fusing point, causing loss of moisture, reduction or oxidation, and the decomposition of carbonates and other compounds

Chelating agent – compound which bonds to metal ions, forming metal complexes

Colloid – a suspension in which the dispersed phase is so small (~1-1000 nm) that gravitational forces are negligible and interactions are dominated by short-range forces, such as van der Waals attraction and surface charges.

Condensation - a chemical reaction in which water or another simple substance is released by the combination of two or more molecules

Diol - compound having two hydroxyl groups added

Gel – a substance that contains a continuous porous solid skeleton enclosing a continuous liquid phase

Gel point - the time at which the last bond is formed which completes the macromolecular gel (the spanning cluster)

Hydrolysis - decomposition of a chemical compound by reaction with water

Inorganic – containing no carbon

Lewis acid – can accept a pair of electrons and form a coordinate covalent bond

Ligand - an ion, a molecule, or a molecular group that binds to another chemical entity to form a larger complex

Metal alkoxide – members of the family of metalorganic compounds, which have an organic ligand attached to a metal or metalloid atom.

Metalorganic – compounds which have an organic ligand attached to a metal or metalloid atom

Mesoporous – materials with very high specific surface area whose pore diameters are in the range 20-500Å

Methoxy (•OCH3) i.e. methoxysilane Si(OCH3)

Nanocomposite – Nanomaterials that combine one or more separate components in order to obtain the best properties of each component

Nanomaterial - synthetic and metastable materials characterized by microstructures in which at least one of their dimensions is less than one hundred nanometers

Nucleophilic attack - an electron-rich nucleophile attacks a molecule and replaces a group or atom

ORMOSIL – organically modified silicate

Organometallic – compounds having direct metal-carbon bonds, not metal-oxygen-carbon linkages

Non-ionic surfactant- a surfactant which has no charge groups on its head and does not dissociate in water

Polymer ("many member") is a huge molecule (a.k.a *macromolecule* formed from hundreds or thousands of units called *monomers* that are capable of forming at least two bonds. An *oligomer* is a molecule of intermediate size – much larger than "mono," but much less than "macro".

Silicate - Any of numerous compounds containing silicon, oxygen, and one or more metals

Sol – a colloidal suspension of solid particles in a liquid

Sol-gel – the preparation of ceramic materials by preparation of a sol, gelation of the sol, and removal of the solvent

Surfactant - wetting agent that lower the surface tension of a liquid, allowing easier spreading, and lower the interfacial tension between two liquids

Xerogel – dried open structure